Pergamon

0306-4522(95)00406-8

Neuroscience Vol. 70, No. 4, pp. 861–891, 1996
Elsevier Science Ltd

0306-4522/96 $15.00 + 0.00

NEURAL DYNAMICS IN CORTEX–STRIATUM CO-CULTURES—I. ANATOMY AND ELECTROPHYSIOLOGY OF NEURONAL CELL TYPES

D. PLENZ*† and A. AERTSEN‡

†Max-Planck-Institut für biologische Kybernetik, Spemannstrasse 38, 72076 Tübingen, Germany
‡Center for Research of Higher Brain Functions, Department of Neurobiology, Weizmann Institute of Science, Rehovot 76100, Israel

Abstract—An *in vitro* system was established to analyse corticostriatal processing. Cortical and striatal slices taken at postnatal days 0–2 were co-cultured for three to six weeks. The anatomy of the organotypic co-cultures was determined using immunohistochemistry. In the cortex parvalbumin-positive and calbindin-positive cells, which resembled those seen *in vivo*, had laminar distributions. In the striatum, strongly stained parvalbumin-positive cells resembling striatal GABAergic interneurons and cholinergic interneurons were scattered throughout the tissue. The soma area of these interneuron classes was larger than the average striatal soma area, thus enabling visual selection of cells by class before recording. Cortical neurons with projections to the striatum showed similar morphological features to corticostriatal projection neurons *in vivo*. No projections from the striatum to the cortex were found. Intracellular recordings were obtained from 94 neurons. These were first classified on the basis of electrophysiological characteristics and the morphologies of cells in each class were reconstructed. Two types of striatal secondary neurons with unique electrophysiological dynamics were identified: GABAergic interneurons ($n = 17$) and large aspiny, probably cholinergic, interneurons ($n = 15$). The electrophysiological and morphological characteristics of cortical pyramidal cells ($n = 27$), cortical interneurons ($n = 1$), as well as striatal principal neurons ($n = 34$), were identical to those reported for similar ages *in vivo*.

Organotypic cortex–striatum co-cultures are therefore suitable as an *in vitro* system in which to analyse corticostriatal processing. The network dynamics, which developed spontaneously in that system, are examined in the companion paper.

Key words: pyramidal neuron, medium-spiny projection neuron, corticostriatal projection neuron, interneuron, development.

Information from the cortex gains access to the basal ganglia at the level of the neostriatum. It has been demonstrated that this strong cortical input[70,121] is crucial for striatal dynamics.[1] Thus, insight into the principles that govern corticostriatal processing is a prerequisite for understanding the cortex–basal ganglia system. However, several features complicate the analysis of corticostriatal processing. Firstly, striatal dynamics depend critically on the level of input activity. Over 90% of the striatum[71,87,119] is comprised of GABAergic,[77,100,112] medium-sized, spiny[21,137,142] projection neurons (principal neurons),[31,95,108,122] which receive excitatory projections from almost all cortical areas.[92] Intracellular *in vivo* studies in lightly anaesthetized animals have shown that, upon cortical activation, striatal principal neurons reach a depolarized, subthreshold state.[138,143] This "enabled state" seems to represent a fundamental operational mode of the striatum. These unique dynamics are highly vulnerable to anesthetics[138] and have not been reported in commonly used *in vitro* approaches, such as the acute brain slice preparation. Secondly, at least two classes of interneurons profoundly influence striatal network dynamics. The GABAergic interneuron[112] takes part in prominent local inhibitory loops as judged from anatomical findings[13,20,35,73] and the cholinergic interneuron is involved in striatal responses to dopamine (DA).[85,94] Together, these classes make up only 3–5% of the cells in the striatum[73,77,107] and, hence, they are difficult to access by chance. Thus, only limited information on their physiological activity is available.[63,65,67,73,141] Thirdly, striatal dynamics most likely operate on an extended spatiotemporal scale. The striatal anatomy is strongly suggestive of a lateral inhibition network,[11,12,108,142]

*To whom correspondence should be addressed. Present address: University of Tennessee, Department of Anatomy and Neurobiology, College of Medicine, 875 Monroe Avenue, Memphis, TN 38163, U.S.A.

Abbreviations: AHP, afterhyperpolarization; ChAT, choline acetyltransferase; DA, dopamine; DiI, 1,1-dioctadecyl-3,3,3,3-tetramethylindocarbocyanine perchlorate; FCS, fetal calf serum; GAD, glutamate decarboxylase; NADPH, reduced nicotinamide adenine dinucleotide phosphate; P, postnatal day; PBS, phosphate-buffered saline; TBS, Tris-buffered saline; TH, tyrosine hydroxylase.

although direct electrophysiological evidence has not yet been reported.[62,64,86,104,109] From theoretical considerations and computer models of lateral, recurrent inhibitory networks,[44,52,53,98,132,135] it is known that on the system level a "winner takes all" dynamics[135] can develop, with additional spatial phenomena such as disinhibitory zones.[132] Thus, besides showing unique temporal features, striatal operation might incorporate spatial complexity as well.[19] Taken together, these features imply that true progress in understanding corticostriatal processing is constrained by the availability of cortical input activity, by the access to striatal interneurons and by the analysis of spatiotemporal dynamics at the system level. To overcome these problems, we have established a new *in vitro* system, the organotypic cortex–striatum co-culture. In such a system the spontaneous activity of the cortical culture is sufficient to drive the striatal network and, moreover, a visual selection of striatal interneurons is possible. These properties potentially make the cortex–striatum co-culture an ideal system in which to study the role of identified neurons in spatiotemporal neuronal network dynamics.

A large body of evidence suggests that the neurotransmitter DA has a strong impact on corticostriatal processing.[20,41,94] To understand the role of DA we first examine cortical and striatal dynamics in the absence of DA. DA is not present since mesencephalic cells are not included in the organotypic co-culture system and the absence of DA was confirmed immunohistochemically. The characteristic corticostriatal dynamics that develop in the absence of DA will then be used as a basis to study the effects of DA at the systems level.

This paper describes the macroscopic organization of the co-cultures and the morphological and electrophysiological characteristics of five different cortical and striatal neuron classes. At least three striatal neuron types were identified by visual inspection of the cell body area before recording. In addition, corticostriatal projection neurons were revealed anatomically. In a companion paper,[107a] we quantitatively analyse the spatiotemporal activity dynamics of the co-culture system using optophysiological and electrophysiological means.

EXPERIMENTAL PROCEDURES

Cortex–striatum co-cultures

Preparation of organotypic cortex–striatum co-cultures. The brains of newborn Sprague–Dawley rats [postnatal days (P) 0–2 colony maintained at MPI für Virusforschung, Tübingen] were removed, the hemispheres were separated and cut transversely at the level of the thalamus. The frontal pole of the brain was removed by a transverse cut at the level of the anterior limit of the caudate–putamen. The hemispheres were then cut in transverse slices (350 μm) on a Vibratome (Campden). For further dissection only slices comparable to coordinates bregma 1.7 to −1.3 from adult rat brains[106] were used. Single tissue pieces from cortex and caudate–putamen (dorsal or dorsolateral) were dissected under a stereomicroscope. This procedure selects cortical tissue pieces mainly from somatosensory cortex and/or primary motor cortex.[54,134] Care was taken to avoid including tissue from the nearby medial agranular or medial precentral cortex[110,131] and medial or medioventral parts of the caudate–putamen and nucleus accumbens.[9] Tissue pieces were placed 0.5–1 mm from each other onto a membrane (Millicell-CM, Millipore PICM) on a coverslip with the striatal tissue, without further specific orientation of the striatal tissue itself, close to the cortical white matter. Co-cultures were embedded and grown according to the roller tube technique[45,46] for three to six weeks. No DA was added.

Quality criteria of co-cultures. Only co-cultures which had no extensive plasma-rips and no brownish center in the cortical part of the co-culture were used. In previous studies, we showed that cortical pyramidal cells in such brownish regions exhibit very broadened spike half widths and a "hump" during the falling phase of the spike. These are characteristics of neurons with a defect in the spike generation system.[61,91]

Fixation and facilitation of penetration. All co-cultures were fixed for 5 min in 4% paraformaldehyde in phosphate-buffered saline (PBS; 0.1 M at pH 7.4) and for 10 min in 4% paraformaldehyde in 0.1 M PBS at pH 11.0. After washing in PBS, co-cultures were incubated overnight in 30% sucrose in PBS. Facilitation of tissue penetration was achieved by shock freezing.

Immunohistochemistry

Immunohistochemical labeling was done according to the biotin–avidin–peroxidase method. For controls, the first antibody was omitted. Negative tyrosine hydroxylase (TH) staining in the co-cultures was controlled by using in addition acute striatal slices from a five-week-old rat.

Parvalbumin. A monoclonal antibody (Sigma, P3171) was used. After fixation and freezing, co-cultures were washed in PBS, preincubated in 2% rabbit serum (Vector, S-5000; PBS, 30 min) and incubated in antiserum (1:1000 in 2% rabbit serum in PBS; 48–72 h at 4°C). After washing, the co-cultures were treated with biotinylated anti-mouse immunoglobulin G (Vector, BA-2000; 1:200 in 2% rabbit serum in PBS; 2 h). Visualization of the stain was achieved using the ABC kit (Vector, Vectastain) with subsequent diaminobenzidine reaction (Vector, Peroxidase Substrate Kit DAB SK-4100). Co-cultures were embedded in glycerin–PBS solution (Citifluor AF1 R1320) and sealed with DePeX (Serva 18243). In some cases a Nissl stain was added.

Choline acetyltransferase. A monoclonal antibody was used (Boehringer Mannheim, 770990). After fixation and freezing, co-cultures were washed in 0.1 M Tris-buffered saline (TBS) at pH 7.4, pretreated with 10% rabbit serum (Vector, S-5000; 1 h) in TBS and incubated in antiserum (1:4 in a mixture of 20% rabbit serum, 2% fetal calf serum (FCS; Sigma, A-7906 in TBS; 48–72 h at 4°C). After washing in TBS, co-cultures were treated with biotinylated anti-rat immunoglobulin G (Vector, BA-4000; 1:70 in a mixture of 20% rabbit serum, 2% FCS in TBS; 2 h). Visualization and mounting procedures were similar to those described for the parvalbumin stain.

Calbindin. The staining was performed in a similar way as for the parvalbumin staining, using an anti-calbindin-D_{28k} monoclonal antibody (Sigma, C8666).

Tyrosine hydroxylase. The immunohistochemical procedure was performed as described previously by several authors,[102,125] except that for facilitation of tissue penetration shock-freezing instead of Triton X-100 was used. The staining was performed with an antibody raised in mice (Boehringer Mannheim, 1017 381). After fixation and freezing, co-cultures were washed in 0.05 M TBS at pH 7.4, pretreated with 10% FCS in TBS for 1 h and incubated in

antiserum (1:600 in 10% FCS in TBS; 48–72 h at 4°C). After washing in TBS, co-cultures were treated with biotinylated anti-mouse immunoglobulin G (Vector, BA-2000; 1:200 in 10% FCS in TBS; 2 h). Visualization and mounting procedures were as described for parvalbumin.

Neuroanatomical reconstruction of recorded cells. Neurobiotin was injected by passing depolarizing current pulses (0.5–1.0 nA, 250 ms, 2 Hz) for at least 15–30 min. The visualization procedure followed previously published protocols.[57,74] In short, co-cultures were fixed and shock-frozen as described for immunohistochemistry. After washing, co-cultures were incubated in fluorescein–avidin D (Vector) and further processed for avidin–biotin–peroxidase staining using the ABC kit (Vectastain) and the diaminobenzidine kit (Vector, SK-4100).

Cell body area statistics. The distribution of striatal cell body areas was based on analysis of Nissl-stained sections. Cell body contours were drawn at ×400 using a phototube and areas were digitized. Quantitative estimation of the cell body area distribution was achieved by using the "square-counting" method: cell bodies completely within a virtual square and cell bodies which cut two previously selected border lines were counted. This corrects for an overestimation of very large-sized cell bodies. To account for shrinkage in the Nissl stain, values gained from dehydrated cell bodies were corrected by 22%.[115]

Anatomical projections. For anatomical tracing using 1,1-dioctadecyl-3,3,3,3-tetramethylindocarbocyanine perchlorate (DiI), co-cultures were fixed for several days in 4% paraformaldehyde in 0.1 PBS, pH 7.4 at 4°C. DiI crystals (Molecular Probes, D-282) were placed into the cortical or striatal part of the co-cultures under stereoscopic control. Co-cultures were stored for at least two months in 4% paraformaldehyde in 0.1 PBS, pH 7.4, at room temperature in the dark. For reconstruction, the fluorescent stain was photoconverted in 2% diaminobenzidine (Serva) in TBS using a rhodamine filter (Zeiss, BP 546, FT 580, LP 590).

Intracellular recordings. For recording, co-cultures were submerged in a recording chamber (total volume *c.* 500 μm). Saturated (95% O_2; 5% CO_2) Hanks' balanced salt solution (Gibco) with 2 mM $CaCl_2$ added was used as extracellular medium. The extracellular concentrations of potassium ($[K^+]_o$), hydrogencarbonate ($[HCO_3^-]_o$) and calcium ($[Ca^{2+}]_o$) were estimated to be 5.8, 4.8 and 2.9 mM, respectively. The flow rate was set to 2–3 ml/min and the temperature was held at 35 ± 1°C. Recordings started after the co-cultures had been left in the new environment for 30–60 min. Often, recordings were done for up to 10 h from a single co-culture without any signs of electrophysiological deterioration.

Intracellular recordings were made using sharp microelectrodes (90–140 MΩ) containing 2 M potassium acetate and 2% neurobiotin (Vector) under visual control (Zeiss IM 35; Zeiss: ×63 Neofluar). The majority of cells had a cell body diameter very much below 20 μm. These cells were considered to be striatal principal cells. Striatal cells were considered to be interneurons if their cell body diameter was larger than 20 μm. Stable intracellular recordings were maintained for 10 min to several hours. Cells were included in the analysis only if intracellular recordings showed (i) an action potential maximum of at least 0 mV, (ii) a stable resting membrane potential and (iii) no cell body swelling. Signals were recorded with conventional electronics made in our institute. Stepwise symmetrical hyper- and depolarizing current pulses (50 ms) were used to construct current–voltage (*I–V*) relationships. Three to six sets of *I–V* measurements were made during phases of low spontaneous activity. Intracellular electrophysiological signals were filtered between 0 and 1 kHz (80 dB/decade), digitized and analysed on a PC (Spike 2, Version 4.0, Cambridge Electronic Design). Curve fitting (sigmoid function; two-exponential decay) was done using conventional PC software (Origin).

RESULTS

Nissl stain

During the first three weeks of culturing, the cortex and the striatum flatten to a thickness of one to three cell layers. Both tissue parts increase in area, and in general the cortical and striatal parts of the co-culture closely approach each other. The cortex mostly showed a kidney-shaped borderline and, in some cases, was slightly thicker in the middle. The striatum reached a homogeneous thickness over the mostly circular extension. At the periphery, faint cell bridges extending into the plasma clot were visible. In contrast to the cortical tissue with its large, pyramidal-shaped cell bodies, the striatal tissue was characterized by its small, mostly circular, cell bodies, with larger cell bodies scattered among them. The borderline between cortex and striatum could be clearly delineated by visual inspection. To facilitate orientation in the co-culture system, the convex border of the cortical culture will be called the "upper border". This region corresponds approximately to layer Ib *in vivo*. The concave border of the cortical culture will be called the "lower border". This region approximately corresponds to layer VI and/or the white matter *in vivo*.

Immunohistochemistry

The aims of the immunohistochemical experiments were (i) to compare the overall organization of the *in vitro* co-culture system with the *in vivo* organization, (ii) to verify the existence of various interneuron classes and (iii) to check for the presence of the DA synthetic enzyme, TH.

Parvalbumin

Parvalbumin is a calcium-binding protein[6] and exists in a number of cortical and striatal GABAergic interneuron classes.[27,30,35,55,78] Furthermore, it has been shown in various species that the distribution of parvalbumin-positive cells is critically dependent on the developmental stage[18,56] and on the activity level.[114,129] Thus, the stain allows for a complex judgment regarding the organization of the co-culture system. We examined 40 co-cultures at 23–26 days in culture.

Cortex. The spatial distribution of parvalbumin-positive cells in the cortex showed a characteristic pattern after three weeks of culturing (Fig. 1A). Parvalbumin-positive cells were found in all areas of the cortical culture. An accumulation of parvalbumin-positive cells was clearly visible in the middle third of the cortex, in which the neuropil shows an intensive staining of dendritic and axonal processes. Cells oriented in parallel to the upper border of the cortex are prominent in this region. In the upper part, bipolar cells were typically oriented perpendicular to the upper cortical border (Fig. 1B). In the lower third of the cortex, besides the existence of bipolar

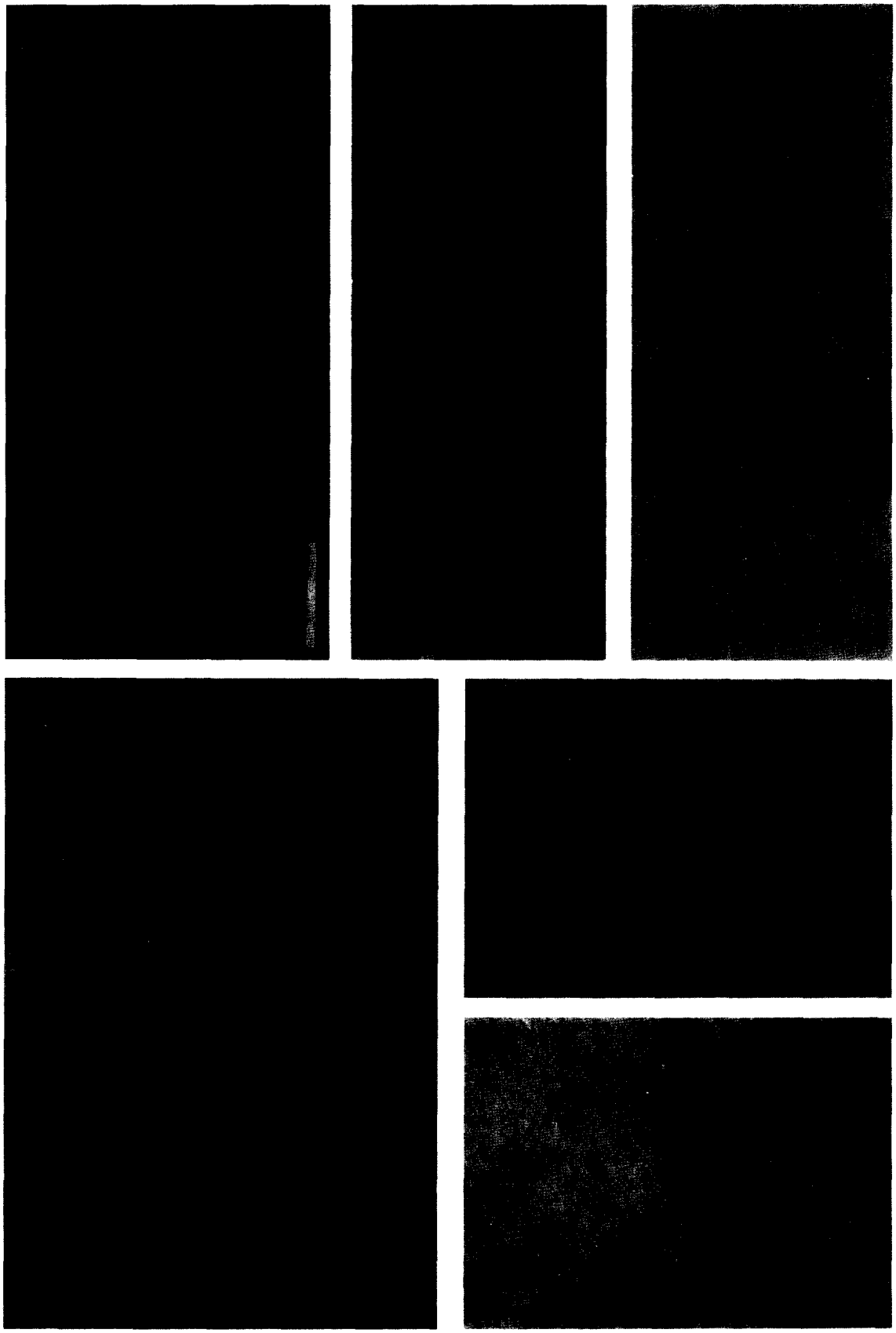

Fig. 1. Parvalbumin-positive cells in the cortical part of cortex–striatum co-cultures. (A) Distribution of cortical parvalbumin-positive cells (24 days *in vitro*, d24). Parvalbumin-positive cells are widely distributed in the upper and lower third of the cortex. A high density of parvalbumin-positive cells is also seen in the lower middle third of the cortical tissue (up: corresponding to supragranular layers *in vivo*; down: corresponding to infragranular layers *in vivo*). (B) Weakly stained bipolar cell from the upper third of the cortex (d25). (C) Strongly stained bipolar cell from the lower third of the cortex (d25). Dendrites with varicosities (arrowheads). (D) Multipolar "basket" cell (d25) with dendritic varicosities (arrowheads). Axonal processes with multiple boutons surround an "imaginary" large cell body ("basket"; arrow). (E) This neuron is an example of triangular cell soma (d25). (F) Parvalbumin-positive fibroblast in the outer region of the cortex culture (d33). Scale bar = 200 μm (A, F); 25 μm (B, C, E); 50 μm (D).

parvalbumin-positive neurons (Fig. 1C), multipolar cells were common (Fig. 1D, E).

The intensity of the stain varied drastically among cells. Bipolar cells from the upper region of the cortex mainly showed staining in the cell body and basal dendrites (Fig. 1B). Cells from the middle and lower part of the cortical culture (Fig. 1C, D) could be reconstructed far into the dendritic and axonal tree. Dendrites were smooth and showed dendritic varicosities (Fig. 1C, D; arrowheads). Multipolar cells were in close proximity to "baskets" (Fig. 1D, arrow). Such "baskets" were formed by axon(s) of strongly parvalbumin-positive multipolar cells and were always situated near the lower border of the parvalbumin-positive layer in the middle third of the cortex. A further cell type was characterized by three primary dendrites, which gives the cell body a triangular appearance (Fig. 1E). Finally, in co-cultures more than four weeks old an increasing number of fibroblasts were present (Fig. 1F).

Striatum. The cultured striatal neuropil was intensively stained by dendritic processes and by axonal processes with "boutons" clearly visible. As the striatal tissue was approximately two-dimensional, most of the dendritic and axonal arborizations of strongly labeled cells could be seen without serial reconstructions. The most prominent cell type was a strongly labeled neuron of fusional-polygonal shape (Fig. 2A). It was distributed homogeneously throughout the striatal culture and its morphology could be traced far beyond the cell body into the dendritic and axonal trees. This cell type was characterized by two to three thick primary dendrites, which branch into several thinner dendrites 50–100 μm from the cell body (Fig. 2A; arrows).

The thinner dendrites generally showed varicosities (cf. Fig. 3A, B, arrows). Darkly stained cells of multipolar and triangular shape were also present (Fig. 2B–D). In the former case, four to nine thick primary dendrites were discerned and the initial part of the axonal tree could be readily reconstructed. The axon branched extensively to form several collaterals at a short distance from the cell body, as well as a number of collaterals far outside the main dendritic tree (Fig. 2B, C, double arrowheads; Fig. 3A, B, ax). In some cases two axons were found (Fig. 3B, ax1, ax2). Often, the axons showed several "boutons" close to unstained, relatively small cell bodies, which stand out from the more brownish neuropil background (e.g. Fig. 3B, open arrows). Throughout the striatal culture, a large number of weakly stained, medium-sized cell bodies, with no further staining in the dendritic and axonal tree, were present. One example is shown in Fig. 2D (right part). Occasionally, neurons with large cell bodies were found, but they were stained only in the cell body and the primary dendrites (Fig. 3C). In addition, large unstained cell bodies, covered by intensively parvalbumin-positive axonal boutons, were seen in a few cases (Fig. 3D). In some cases the total number of weakly and strongly parvalbumin-positive cells in the striatal part of the co-culture was very low. Twenty to thirty percent of co-cultures showed only very low numbers ($n = 3$–10) of strongly labeled cells in the striatum. These reductions in the striatal parvalbumin stain were not paralleled in the cortical tissue, which always showed very intense staining.

Choline acetyltransferase

Choline acetyltransferase (ChAT), the synthetic enzyme for acetylcholine, is a marker for cholinergic neurons in the CNS.[37,43] In rats, striatal ChAT-positive cells first appear in the third postnatal week.[51] To find if cholinergic neurons develop in the co-culture system we examined 30 co-cultures for ChAT immunoreactivity after 18–35 days *in vitro*.

Cortex. In one case four ChAT-positive cell bodies were present in the cortex. The morphology of these neurons was similar to the ChAT-positive cells in the striatal part.

Striatum. In all co-cultures ChAT-positive cells were widely distributed in the striatal part. Occasionally, multiple central areas of the tissue were devoid of ChAT-positive cells (Figs 2E, 5B). In three cases cells were restricted to a small striatal region. Often, labeled cells were found in striatal cell bridges outside the main striatal region (Fig. 5B). The morphology of ChAT-positive cells appeared to be remarkably homogeneous and was characterized by a large, elongated cell body with three to four long and smooth primary dendrites. The dendritic arborization was generally sparse (Figs 2E, F, 3E). Morphologically, these cells resembled electrophysiologically identified type II neurons (see below). They differed considerably from cells with "principal cell"-like morphologies (Fig. 2F).

Calbindin

Calbindin belongs to the same group of calcium-binding proteins as parvalbumin.[6] The calbindin immunoreactivity was used to characterize further the macroscopic organization in the cortex–striatum co-culture system. Roughly speaking, the distributions of parvalbumin- and calbindin-positive cells in the cortex and the striatum *in vivo* are complementary.[28,116] According to this and the results of the parvalbumin stain in the co-culture system, calbindin-positive cells should be present mainly at the borders of the tissue parts. We examined 33 co-cultures after 23–28 days *in vitro*.

Cortex. Strongly stained cells were predominantly situated at the upper border of the cortex and in the region between the cortex and the striatum (Figs 4A, 5C). Cells were characterized by a fusional-elongated cell body and a very large dendritic tree without spines. In some cases varicosities were present. The neuropil of the cortex was intensively stained with axonal processes showing boutons.

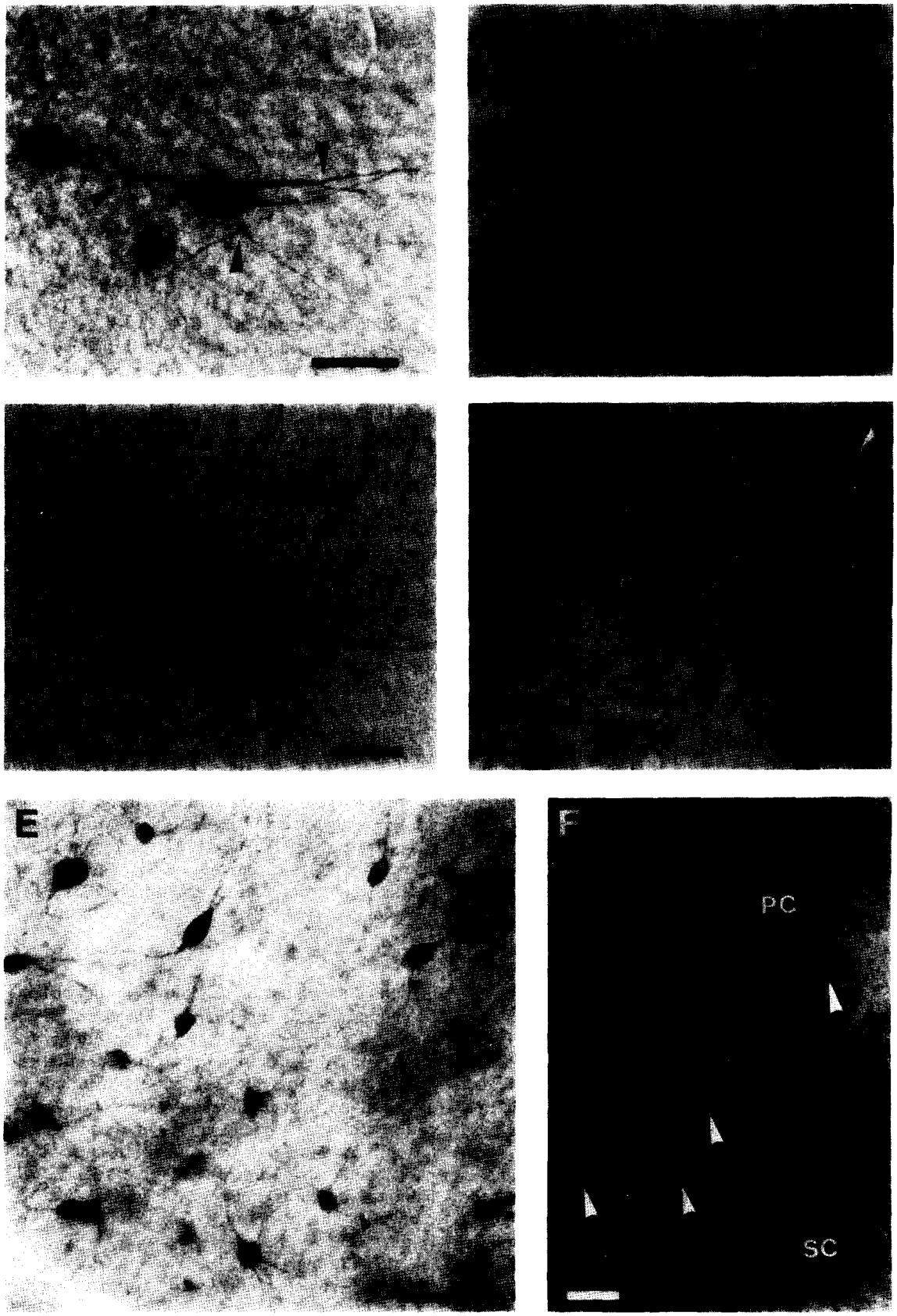

Fig. 2. Immunohistochemical cell types in the striatal part of cortex–striatum co-cultures. (A) Common parvalbumin-positive cell type with thick primary dendrites, which branch off into several thin processes at a short distance from the cell body (24 days *in vitro*, d24; arrowheads). (B) Multipolar parvalbumin-positive cell (d24) has a round cell body. Its initial axon segment (double arrowheads) and dendritic varicosities are clearly visible (arrowhead). (C) A multipolar polygonal parvalbumin-positive cell with the axon clearly visible (d24; double arrowheads). Axon branching is characterized by triangular plates. (D) A parvalbumin-positive cell with a triangular-shaped cell body. (E) ChAT-positive cells (d23). (F) Comparisons between ChAT-positive cells and neurobiotin-filled neurons (d21). A secondary type Ib cell with "principal-cell"-like (PC) morphology and a secondary type II cell (SC) with the typical morphology of striatal ChAT-positive cells (arrowheads) are shown. Scale bar = 25 μm (A–D); 50 μm (E, F).

Striatum. In the striatal part of the co-culture, calbindin-positive cells were found only occasionally (Fig. 4B). In most cases, these cells were restricted to the border of the striatal tissue (Fig. 5C). The striatal neuropil was devoid of strongly labeled dendritic and axonal processes. However, many weakly stained

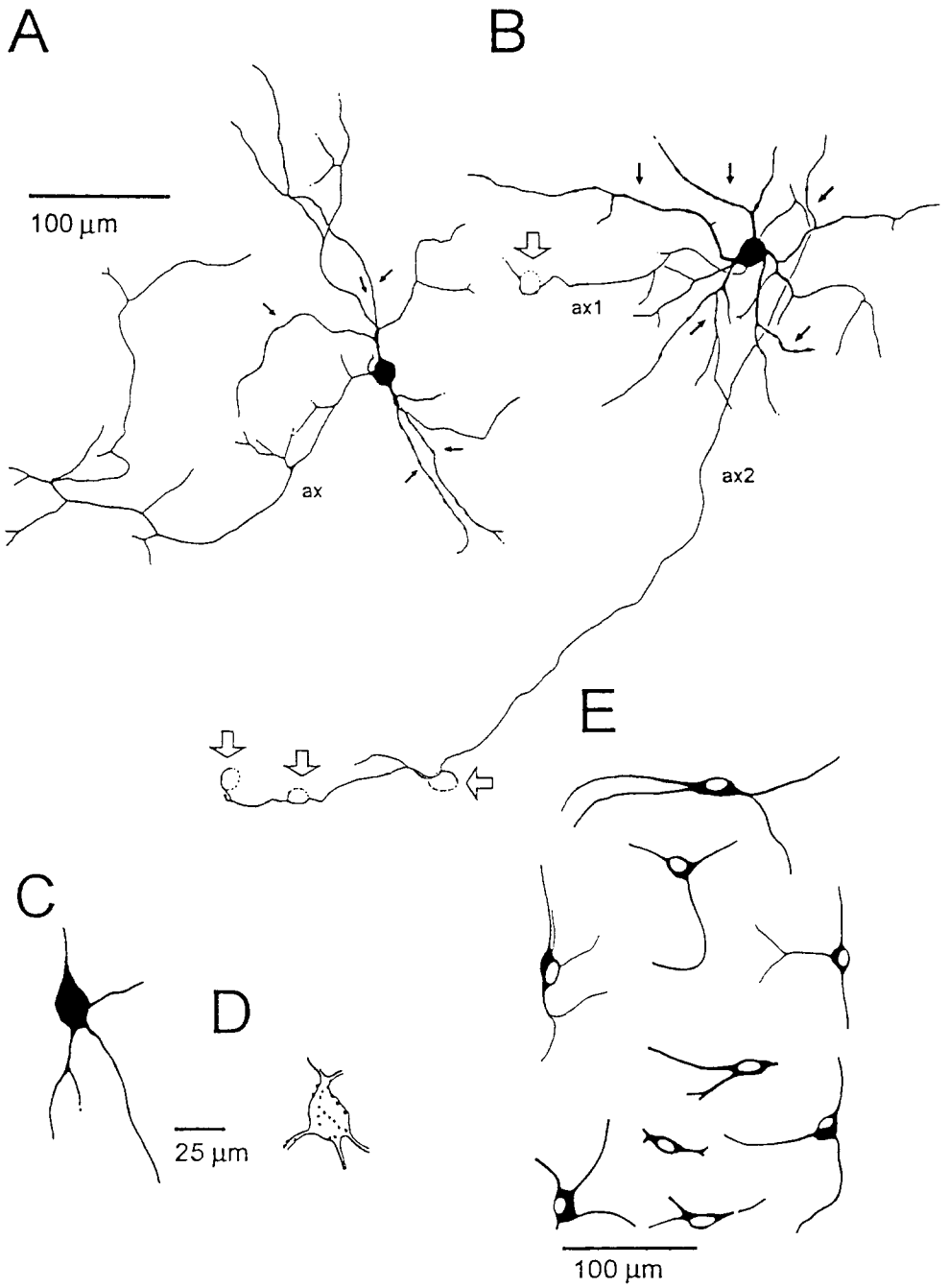

Fig. 3. Reconstruction of striatal parvalbumin- and ChAT-positive cell types. (A) Commonly found strongly stained bipolar parvalbumin-positive cell type. At a short distance from the cell body thick primary dendrites abruptly branch off into several thin dendrites which have dendritic varicosities (arrows). The main axon (ax) branches off several times in close vicinity to the cell body and then takes a course outside the main dendritic field. (B) Parvalbumin-positive cell similar to that described in A. Note that this neuron possesses three thick primary dendrites and two axons (ax1, ax2). The axons (ax1, ax2) show an increased density of boutons in proximity to parvalbumin-negative cells (open arrows). (C) A large, polygonal cell body and tapered primary dendrites distinguish this strongly labeled parvalbumin-positive neuron from the commonly found strongly labeled cell type. (D) Large, parvalbumin-negative cell body surrounded by strongly parvalbumin-positive axonal boutons. (E) ChAT-positive cells in the striatum (rearranged).

Fig. 4. Calbindin-positive cells in cortex–striatum co-cultures. (A) Cells at the upper cortical border. (B) Cell at the striatal tissue border close to the cortical tissue. Scale bar = 25 μm (A, B).

medium-sized cell bodies were present. Given the varying thickness of the whole mount preparation, no patchiness of the striatal neuropil could be seen.

The overall distributions of the interneuron classes examined in the co-culture system can be summarized as follows: parvalbumin-positive neurons showed a distinct lamination in the cortex and were scattered throughout the striatum (Fig. 5A). On a macroscopic scale the distribution of parvalbumin-positive cells is inversely related to the distribution of calbindin-positive cells (Fig. 5A, C). Cholinergic cells were mainly restricted to the striatal tissue part (Fig. 5B).

Cell body area distributions

Cell body area distributions in the striatal tissue part were based on four co-cultures at a given age for each stain (Fig. 5D). The Nissl stain demonstrates that the majority of neurons are small cells with a somal area of $124 \pm 58\ \mu m^2$ (Fig. 5D, upper diagram; 23 days *in vitro*; corrected for shrinkage). From this an average cell body diameter of $11 \pm 8\ \mu m$ was calculated. The average somal areas of ChAT-positive neurons ($327 \pm 99\ \mu m^2$; Fig. 5D, middle diagram; 22 days *in vitro*) and strongly parvalbumin-positive neurons ($327 \pm 64\ \mu m^2$; Fig. 5D, lower diagram; 25 days *in vitro*) were much larger than the somal areas for the majority of striatal neurons. These analyses of the co-culture system prove that the adoption of the visual selection criterion of "neuronal somata having at least one axis of the somatic diameter in the range of 20 μm or above" strongly favors intracellular recordings from cholinergic and GABAergic striatal interneurons.

The co-cultures were grown in the absence of DA. As the main sources for striatal DA are known to reside in regions outside the neostriatum,[47] no dopaminergic activity was expected to exist in the co-culture system. However, two reports of monoaminergic, TH-positive cells in the rat striatum *in vivo* and in organotypic striatal cultures do exist.[102,125] To check for dopaminergic sources intrinsic to the co-culture system, we performed immunohistochemical staining for TH using 11 co-cultures cultured for 23 days *in vitro*. No TH-positive cells were found in the cortical or striatal part of the co-cultures. We conclude that the co-cultures develop under conditions of DA deficiency.

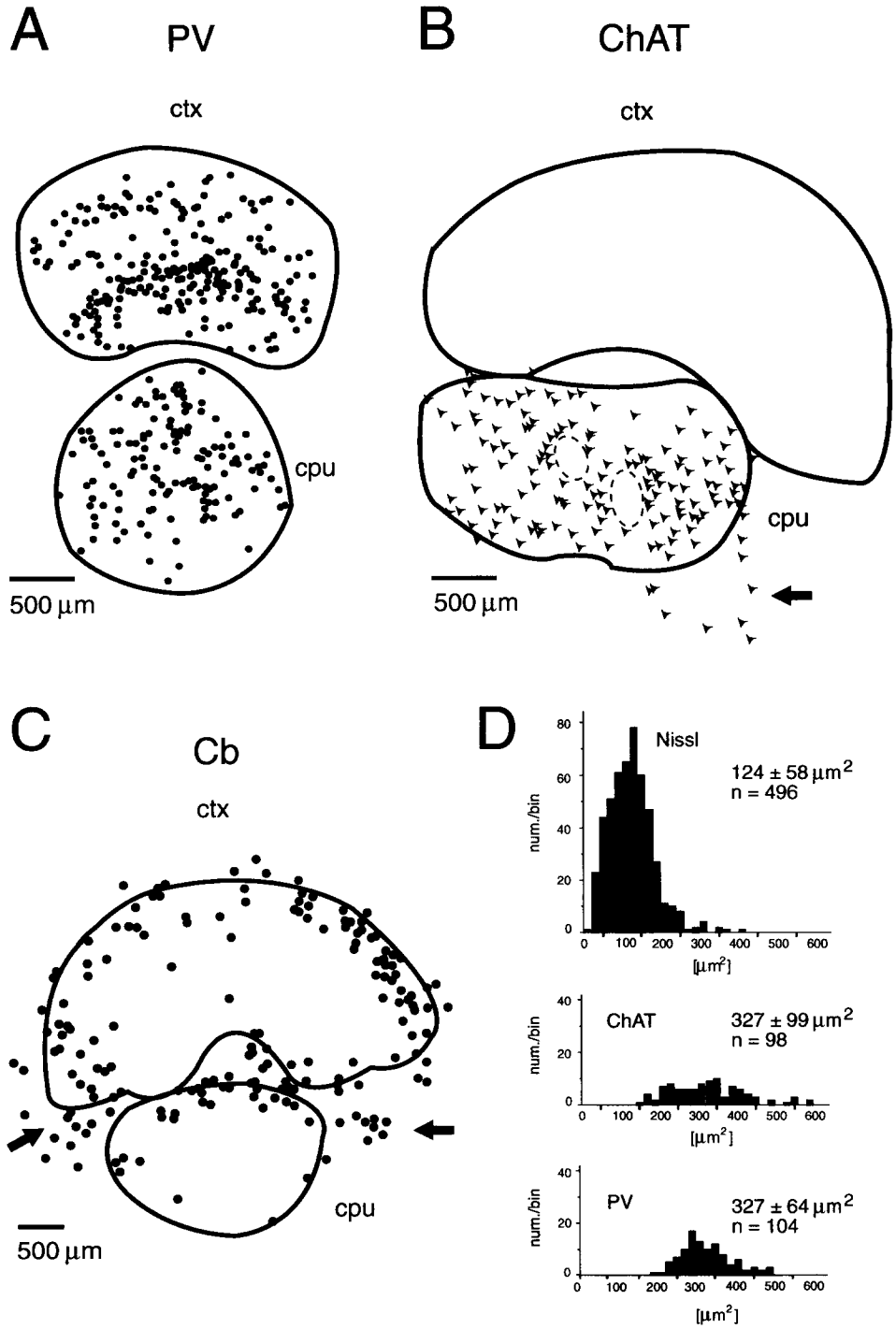

Fig. 5. Distribution of immunohistochemically characterized cell types in the cortex (ctx)–striatum (cPu) co-cultures and estimated striatal cell body area distributions. (A) Distribution of parvalbumin-positive cells (PV) (25 days *in vitro*, d25). Only neurons showing parvalbumin-labeling in the cell body and at least in the primary dendrites are marked. Note the laminar distribution of cortical cells. (B) Distribution of ChAT-positive cells (d22). ChAT-positive cells are restricted to the striatal part. In some cases cells were found outside the main tissue region (arrow). The ellipsoids indicate large regions within the striatal tissue devoid of labeled cell bodies. (C) The distribution of calbindin-positive cells (d24) is complementary to the distribution of parvalbumin-positive cells. (D) Comparison of the cell body area distributions of different striatal cell populations. From the Nissl stain (Nissl, d23) a narrow distribution of small cells with a cell body area of $124 \pm 58\ \mu m^2$ is revealed. Cholinergic (ChAT, d22) and strongly parvalbumin-positive cells (d25) fall in the upper region of striatal cell body sizes.

Corticostriatal projection neurons

To reveal neuronal projections established in culture, we used DiI.[48,127] Massive injections were made into the cortical (21 ± 3 days *in vitro*; $n = 11$) or striatal (22 ± 4 days *in vitro*; $n = 14$) part of fixed co-cultures. After two months, it was always possible to obtain positive labeling in the cortex when DiI had been injected into the striatal part. The cortical neuropil was intensively stained by labeled axonal and dendritic processes. Labeled neurons could be traced long distances along their dendritic and axonal trees and were considered to be neurons projecting to the striatal tissue. The number of such intensively stained neurons varied considerably from stain to stain from 10 to over 40 neurons. For morphological reconstruction of labeled neurons, the fluorescent dye was photoconverted into a dark, stable stain (see Experimental Procedures).

Cell bodies of retrogradely labeled cells in most cases were confined to a horizontal band in the lower part of the cortex (Fig. 6A). All labeled cells possessed dendritic spines and were of pyramidal shape (Fig. 6B, C). The basal dendritic trees were locally restricted (compare Fig. 6B with Fig. 9D). The apical dendrite appeared to be sparsely branched and did not arborize extensively near the upper cortical border (Fig. 6B, C). The detailed morphology and axonal projections of a corticostriatal projection cell were reconstructed (Fig. 6B). The projection neuron was a pyramidal cell and showed several noteworthy features concerning its axonal tree. The main axon was heading straight towards the striatum. One axonal collateral ran along the horizontal extent of the cortex and a second collateral ran parallel to the projection axon down to the lower cortical border. Two other collaterals were heading directly towards the upper cortical border.

No cultures, over a period of two years, showed retrograde transport of DiI from the cortical to the striatal tissue. Thus, we conclude that in the co-culture the flow of activity is directed from the cortex to the striatum.

Electrophysiology and morphology of neuron classes

Five neuronal classes were identified electrophysiologically in the co-cultures (Table 1). The criteria leading to the various cell classes themselves will be explained in detail during the discussion of each single class. The neurons were examined on average at the beginning of the fourth postnatal week. Except for striatal type II neurons, no significant correlations ($r > 0.5$; linear regression) of the parameters with age were observed.

We will first consider the characteristics of the two main cell classes in the cortical and the striatal cultures. Striatal principal cells were significantly more polarized than cortical pyramidal cells and had a lower membrane time constant ($P < 0.005$; t-test). Both classes had a rectification ratio larger than one, with significantly larger values in striatal principal cells ($P < 0.005$; t-test). Pyramidal cells and striatal principal cells were remarkably similar with respect to input resistance, threshold and action potential wave form: no significant differences were found ($P < 0.05$; Wilcoxon's rank sum test).

In the striatal tissue, type Ia and II neurons had the highest resting membrane potential, while principal cells had the lowest. Type Ia and II cells did not differ in their average resting membrane potential ($P < 0.05$; Wilcoxon's rank sum test; see also Fig. 7B). Type Ib neurons took an intermediate position among the striatal classes. The membrane time constant for principal cells was shorter than for type Ia and II cells, but similar to the membrane time constant of type Ib neurons ($P < 0.05$; Wilcoxon's rank sum test). Strong differences were found between the striatal cell classes regarding the steady-state non-linearities. Whereas striatal type II neurons showed linear steady-state dynamics, striatal principal neurons showed a rectification ratio very much larger than one. Striatal type Ia neurons showed a strong outward rectification in the subthreshold range, leading to a quotient less than one. Striatal type Ib neurons showed a unique sigmoid steady-state membrane behavior. For this type of non-linearity, the steady-state dynamics were described using a hyperbolic tangent (Table 2). The threshold was similar in all cell classes ($P < 0.05$; Wilcoxon's rank sum test). The spike width was significantly longer for principal neurons than for secondary neurons ($P < 0.001$; Wilcoxon's rank sum test). These differences in spike widths between principal and secondary cells were due to significant differences in the action potential falling rate ($P < 0.0005$; t-test). The spike width of type II neurons was significantly longer than for type I neurons ($P < 0.05$; t-test). In contrast to striatal principal cells, secondary cells expressed a prominent afterhyperpolarization (AHP) with a maximum hyperpolarization of -12 mV. The time to the maximum AHP amplitude was significantly shorter for type Ia and Ib neurons than for type II neurons ($P < 0.05$; t-test).

Although only one cortical interneuron was recorded, the position of this interneuron among the various cell classes can be considered. A high resting membrane potential, a rectification value smaller than one, a small spike width, the value of the ratio between maximum rise and fall of spike and the prominent AHP show this neuron to be similar to striatal type I cells.

Resting membrane potential and threshold

A comparative analysis of the position each class occupies within the network dynamics was carried out. Our first approach was to plot the resting membrane potential against the absolute threshold for each type of neuron. The result of this analysis is shown in Fig. 7. In Fig. 7A it can be seen that cortical neurons behave as if their resting and threshold

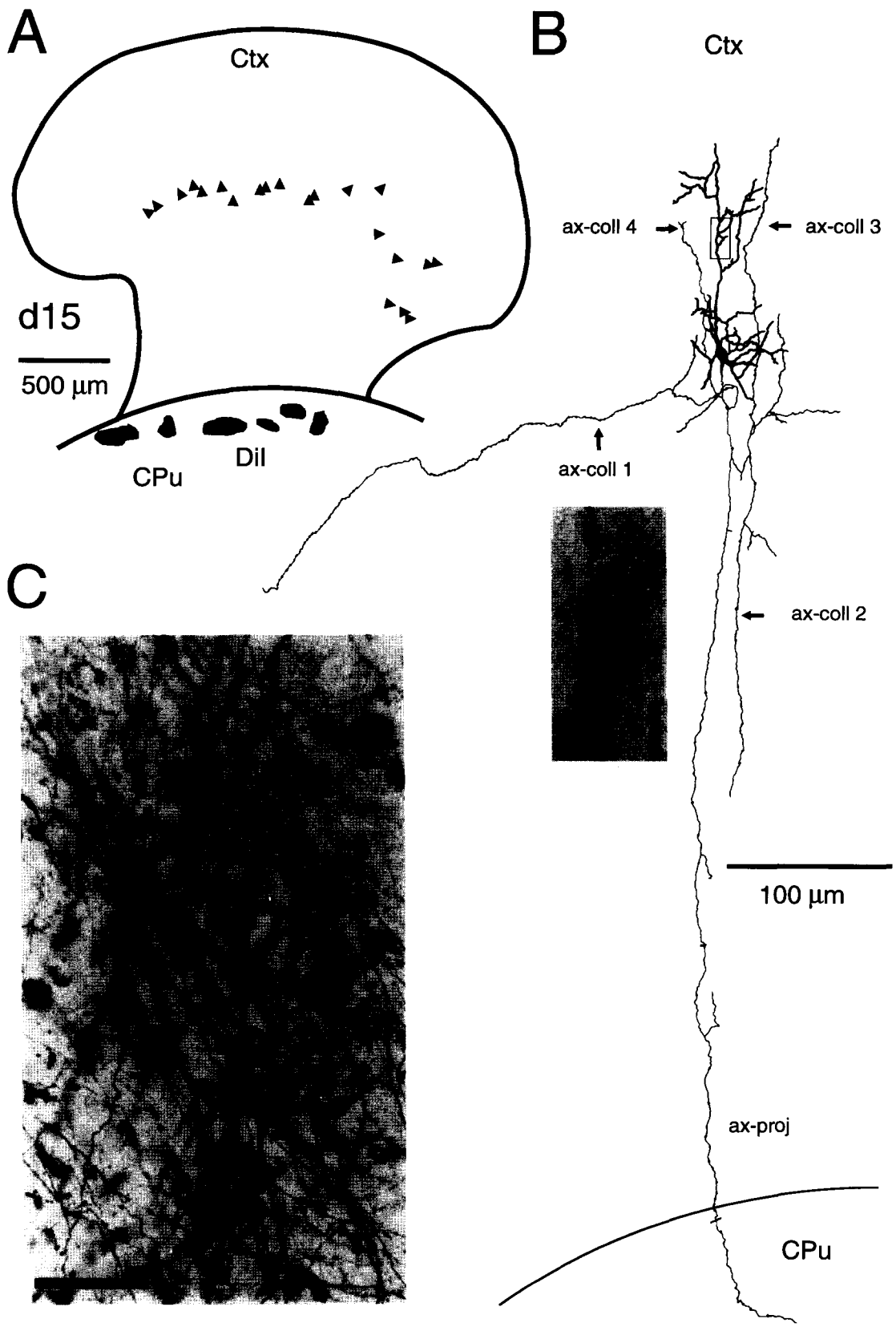

Fig. 6. Corticostriatal projection neurons in cortex–striatum co-cultures. (A) Distribution of corticostriatal projection neurons (15 days *in vitro*, d15) revealed by DiI injections into the striatal tissue (DiI, CPu). The projection neurons are arranged in a horizontal band in the lower part of the cortical culture (Ctx). (B) Anatomical reconstruction of the dendritic morphology, the main axon, which was followed into the striatum (ax-proj), and axonal collaterals (ax-coll) of a corticostriatal projection neuron. Inset shows the presence of dendritic spines. (C) Projection neuron from A with the pyramidal-shaped cell body and spiny dendrites clearly visible. The neuropil shows a high abundance of labeled axons. Scale bar = 5 μm (B, inset); 50 μm (C).

potentials were unrelated. The resting potentials occupied the complete range from more than 20 mV to only a few millivolts from threshold. In the striatal network, a similar range of resting membrane potentials was covered by principal and secondary neurons together. However, a strong negative correlation was found between the resting potential and the absolute threshold, which is connected to the division among different cell classes. Whereas principal cells were situated far away from threshold, type Ia and II striatal interneurons were close to threshold. The class of type Ib secondary neurons is distributed over the complete range covered by the other classes.

Cortical pyramidal neurons

During the first postnatal weeks there is a prominent maturation of the morphological and electrophysiological parameters of cortical neurons *in vivo*.[91] Thus, we examined the maturation of cortical neurons in the co-culture system.

The electrophysiological and morphological characteristics of cultured cortical pyramidal neurons are summarized in Figs 8 and 9. Figure 8 illustrates the electrophysiological characteristics of the most commonly found type of pyramidal neuron. In all of these neurons inward rectification typical of pyramidal neurons was seen. This rectification appeared by the end of the third week and was clearly expressed after the fourth week in culture (Fig. 8A). Further characteristics refer to the change in AHP of the first spike (Fig. 8B). At the end of the fourth week a short afterdepolarization preceded the AHP (Fig. 8C, arrow). The membrane potential decay from subthreshold and suprathreshold levels was fitted by one exponential (Fig. 8D). In three cases rectification in the very hyperpolarized range was revealed (Fig. 9A). These neurons also showed prominent rebounds and hyperpolarizations at the end of hyper- and depolarizing current injections, respectively (Fig. 9B, arrow). Relatively young cortical neurons showed a prominent burst AHP (Fig. 9C). All reconstructed cortical cells ($n = 12$), which showed the electrophysiological characteristics mentioned, were identified as pyramidal neurons. In Fig. 9D, a pyramidal neuron from the upper cortical region is reconstructed. The axon collaterals of this neuron showed a termination field

Table 1. Neuron classes in cortex–striatum co-cultures: electrophysiological characteristics

	Cortex		Striatum			
				Secondary		
	Pyramidal cell	Interneuron	Principal cell	type Ia	type Ib	Secondary type II
age (days)	22 ± 5	18	23 ± 5	23 ± 3	22 ± 3	
um (mV)	−57 ± 5	−49	−62 ± 3	−50 ± 4	−58 ± 6	−53 ± 5
rm* (MΩ)	69 ± 25	25	57 ± 20	63 ± 30	48 ± 24	56 ± 29
tau† (ms)	12 ± 3	7	6 ± 2	9 ± 3	7 ± 2	9 ± 2
rect‡	1.5 ± 0.5	0.6	6.4 ± 3.2	0.65 ± 0.2	—	1.1 ± 0.4
thr§ (mV)	−44 ± 7	−40	−48 ± 4	−44 ± 5	−47 ± 7	−45 ± 6
ap‖ (mV)	65 ± 8	54	65 ± 6	56 ± 10	62 ± 9	61 ± 6
apw¶ (ms)	1.6 ± 0.4	1.0	1.5 ± 0.4	0.7 ± 0.1	0.7 ± 0.1	0.9 ± 0.2
ri (V/s)	63 ± 21	54	63 ± 18	83 ± 20	74 ± 25	81 ± 24
fa (V/s)	−23 ± 10	−47	−28 ± 13	−63 ± 32	−55 ± 18	−50 ± 24
ri/fa	3.0 ± 0.9	1.1	2.5 ± 0.7	1.6 ± 0.4	1.3 ± 0.2	1.8 ± 0.6
AHP** (mV)		−7.5		−12 ± 3	−11 ± 3	−12 ± 3
AHPt†† (ms)		1.4		2.4 ± 0.6	2.1 ± 1.0	3.7 ± 1.4
cell num	27	1	34	9	8	15

Data are taken as mean ± S.D.: age, days cultured *in vitro*; um, resting membrane potential; rm, input resistance; tau, membrane time constant; rect, non-linearity in steady-state response; thr, spike threshold; ap, spike amplitude; apw, half width of spike amplitude; ri, maximum rising rate of spike; fa, maximum falling rate of spike; ri/fa, ratio between maximum rise and fall of spike; AHP, amplitude of spike afterhyperpolarization; AHPt, time to AHP; cell num, number of cells examined.

*Linear regression analysis within ±5–10 mV deflection from resting membrane potential.

†Calculated from responses to weak hyperpolarizing current injections (50 ms).

‡Ratio between the apparent steady state input resistances measured just below threshold and at −20 mV hyperpolarized state.

§Measured using depolarizing current pulses from resting potential. The resting membrane potential minus the minimal depolarization necessary to elicit a spike was taken as absolute threshold value.

‖Measured from resting potential to spike peak.

¶On average, 100–200 spontaneously occurring action potentials were averaged for each cell. The beginning of an action potential was defined by the time point, when the rising rate exceeds 20% of the maximum value.

**On average, 100–200 spontaneously occurring action potentials were averaged for each cell. Under such conditions only in some classes could a clear AHP be delineated. The amplitude difference between the beginning of a spike (see ¶) and the peak spike after hyperpolarization was taken as the AHP amplitude.

††Calculated as the time from spike peak to the AHP.

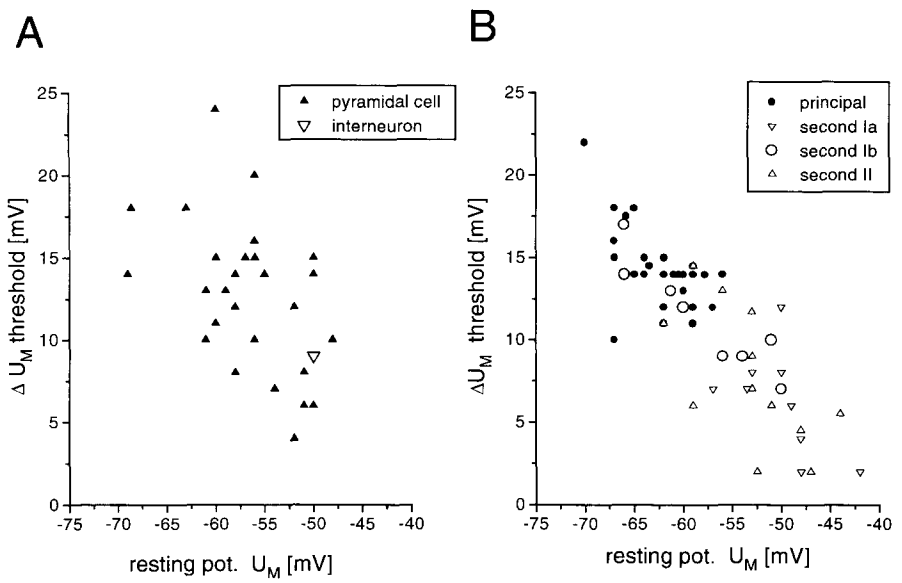

Fig. 7. Distribution of the resting membrane potential and threshold for cortical (A) and striatal (B) neurons in the cortex–striatum co-culture system.

in the same cortical layer 200 μm away from the soma. A pyramidal neuron from the lower cortical region is shown in Fig. 9E.

Cortical interneurons

The neuron was located in the lower half of the cortical tissue. The current–voltage plot was characterized by a strong outward rectification in the subthreshold range (Fig. 10A). Other features of this neuron included vigorous bursting; the membrane potential decay from depolarized levels was best fitted by two exponentials (Fig. 10B, C). The action potentials were followed by prominent AHPs. The neuron had smooth, varicose dendrites and a densely branched local axonal field (Fig. 10D).

Striatal principal cells

Thirty-four neurons were identified as principal cells by the presence of an anomalous rectification at hyperpolarized levels and the absence of outward rectification in the subthreshold range (Fig. 11A). In these neurons, the decay of the membrane potential from subthreshold and suprathreshold depolarized states was best fitted by a single exponential (Fig. 11B). In contrast to this, when tested the relaxation from hyperpolarized levels clearly revealed the existence of an additional fast process having a time constant below 2 ms (1.8 ± 0.4 ms; $n = 4$; Fig. 11B). Reconstructed cells showed a cell body area of 116 ± 26 μm^2 ($n = 10$), which matches the cell body area of the majority of cells in the striatal culture (Fig. 5D). Four to five primary dendrites gave rise to a dendritic tree of circular or ellipsoidal shape (Fig. 12). The dendrites were densely covered with spines (Fig. 12B). In contrast to the situation *in vivo*, the dendrites also showed very proximal spine-like protrusions. The axonal field largely overlapped with the dendritic field.

Striatal secondary type I neurons

Nine neurons showed (i) an outward rectification in the subthreshold range (Fig. 13A) and (ii) a slow component of membrane potential relaxation from depolarized levels (Type Ia; Fig. 13A, B). A further eight neurons also possessed an additional inward rectification at hyperpolarized levels (Type Ib; Fig. 13C, D). Both types did not differ significantly in other electrophysiological parameters, except that type Ib neurons included very polarized cells, leading on average to a more polarized resting potential (Fig. 7B; Table 1).

The membrane potential decay from depolarized levels showed the presence of at least two time components (Fig. 13B, D). After a spike, the time constant of the secondary, slow component increased (Fig. 13C, D). Table 3 summarizes these findings. In two cases the secondary, slow component was only revealed after a spike. In three type Ib neurons the time constant for the secondary, slow process increased to approximately half a second after a burst.

Table 2. Average current–voltage steady-state relationship in secondary type Ib neurons $[y(x) = (A_1 - A_2)/(1 + \exp((x - x_0)/dx) + A_2)]$

	A_1 (mV)	A_2 (mV)	x_0 (nA)	dx (nA)	χ^2
Secondary type Ib ($n = 8$)	-23 ± 9	19 ± 7	-0.04 ± 0.03	-0.13 ± 0.04	-0.22 ± 0.19

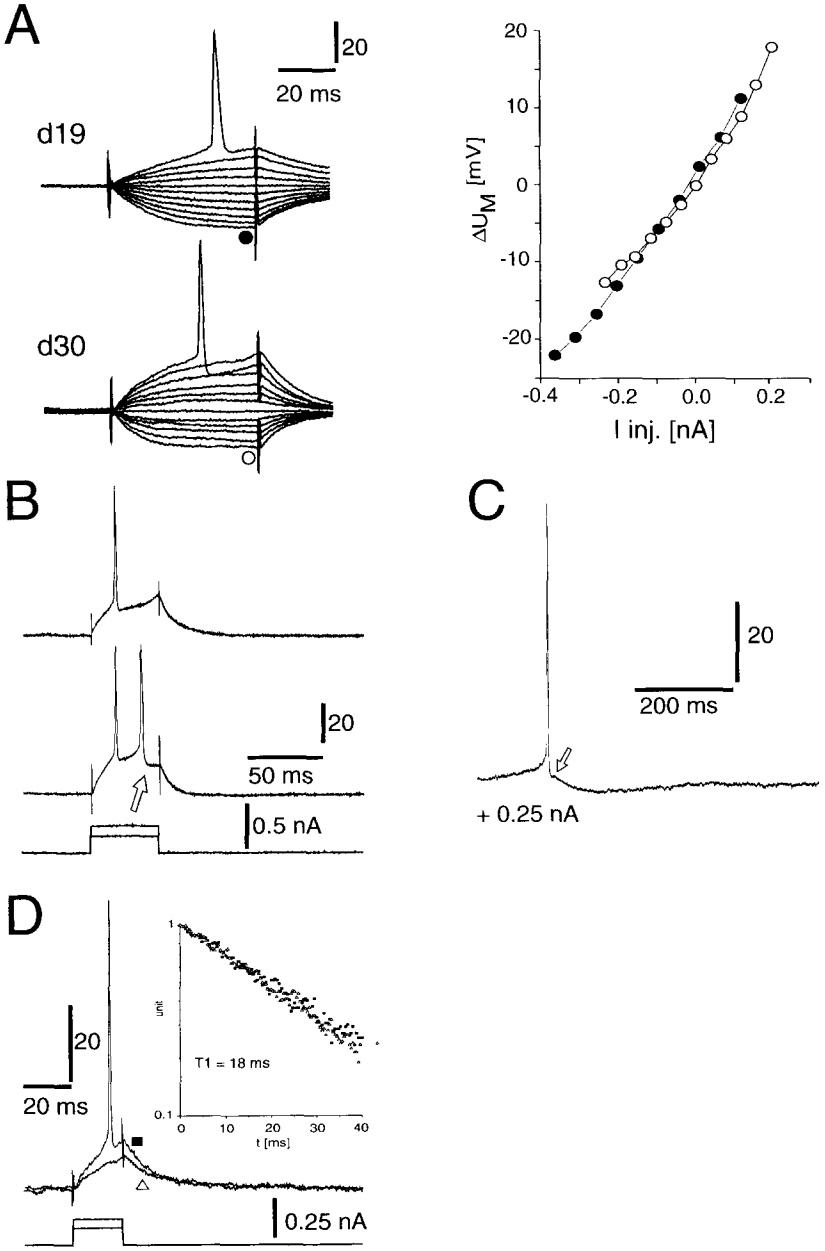

Fig. 8. Electrophysiological characteristics of the most commonly seen cortical pyramidal neuron class in cortex–striatum co-cultures. (A) Passive and active intracellular membrane potential responses. Hyperpolarizing and depolarizing current pulses with equidistant amplitudes were injected into the cell body. Membrane potential values reached after 50 ms were plotted against the subthreshold current amplitudes used (right). (B) Change in AHP after the first spike (arrow). (C) Cortical pyramidal neurons at the end of four weeks in culture show a short-lasting depolarizing "hump" (arrow) during the spike AHP. (D) The decay time course after a sub- and suprathreshold current injection is tested for different components using a semilogarithmic plot for the first 40 ms.

Upon slight increases in current injection, type I cells fired in bursts (Fig. 13A), which often showed spike cessation (Fig. 15A; see also the companion paper). Morphological reconstructions revealed a cell body area of $292 \pm 60\ \mu m^2$ ($n = 6$) and three to six thick primary dendrites with varicosities on higher order dendrites, and no spines (Fig. 14). Axonal termination fields were found several hundreds of micrometers beyond the dendritic field (Fig. 14B, open arrows).

One type Ib neuron closely resembled a principal neuron with respect to morphology. It was located well within the striatal culture and showed a medium-sized cell body, an asymmetric dendritic field and thin dendrites with spines faintly visible (Fig. 2F, PC; Fig. 14C). Its high likelihood of being a principal

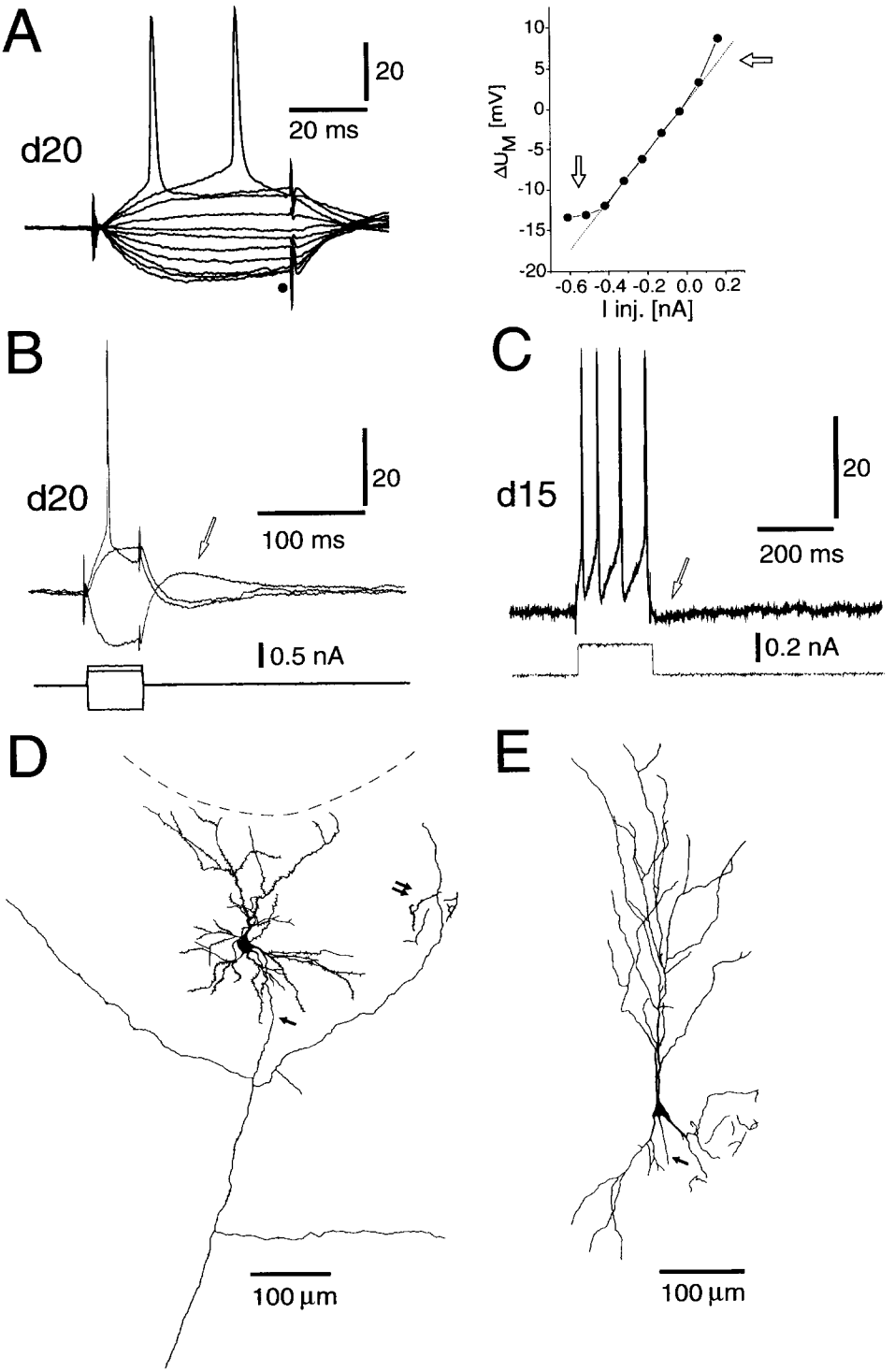

Fig. 9. Electrophysiological characteristics of a second class of pyramidal neurons in cortex–striatum co-cultures and general morphological characteristics. (A) Passive and active intracellular membrane potential responses. Membrane potential values reached after 50 ms were plotted against the current amplitudes used (right). At very hyperpolarized levels an inward rectification is revealed. (B) Hyper- and depolarizing current injections result in typical rebound and hyperpolarization of the membrane potential, respectively. (C) In young neurons strong burst AHPs are present. (D) Morphology of a pyramidal neuron from the upper part of the cortex. Apical and basal dendrites are covered with spines. The axon (arrow) emanates from the cell body and gives off several collaterals, one of them showing terminal branching at a distance of approximately 200 μm at the same cortical depth. (E) Reconstruction (neurobiotin) of a pyramidal cell localized in the lower part of a cortical culture (spines are not drawn).

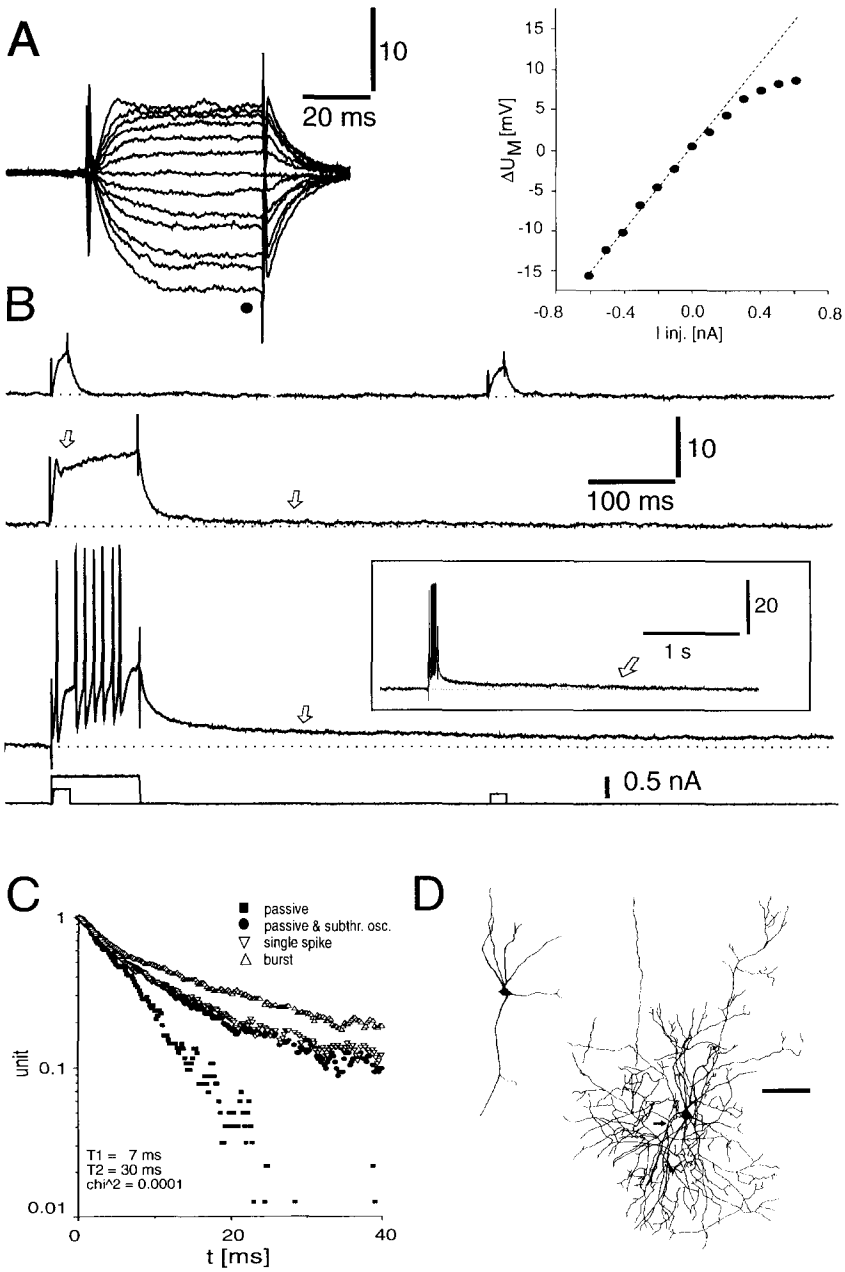

Fig. 10. Electrophysiological and morphological characteristics of a cortical interneuron in the cortex–striatum co-culture (18 days *in vitro*, d18). (A) Intracellular membrane potential responses to hyperpolarizing and depolarizing current pulses with equidistant amplitudes. Membrane potential values reached after 50 ms were plotted against current amplitudes used (right). Linear regression (dotted line) was calculated based on the first four hyperpolarizing membrane potential values viewed from the resting potential. The neuron shows a strong outward rectification in the subthreshold range. (B, C) The responses (upper traces) change with respect to current injections (lower traces). Short-lasting, subthreshold depolarizing current pulses lead to a quick decay to the resting potential after the pulse. Long-lasting subthreshold current injections lead to a short-lasting subthreshold oscillation and a long-lasting decay (arrow). A slight further increase of current amplitude induces a strong spike burst with even longer lasting decay. Note the increased delay between the first and the second spikes compared to the following spike intervals. Inset shows the complete response. All experiments were done shortly after a local blockade of non-*N*-methyl-D-aspartate receptors using 6-cyano-7-nitroquinoxaline-2,3-dione. (C) Semilogarithmic display of the membrane potential decays after depolarizing current pulses. (D) Reconstruction (neurobiotin) of the cortical interneuron localized in the center of the cortex. The thick proximal axon trunk (arrow) emanates from the cell body. Scale bar = 100 μm.

neuron was further supported by its very strong inward rectification (Fig. 13C) and its very low time constant for the slow component ($T2 = 28$ ms; compare Table 3). As most visualized type I neurons resembled strongly parvalbumin-positive neurons in the co-culture system, we conclude that type I neurons are likely to be striatal GABAergic interneurons.

The spiking characteristics for both Ia and Ib neurons included bursting and spike cessation (Fig. 15A, B; see also the companion paper). During the spike cessation the membrane potential was governed by intrinsic currents. Spontaneous input activity resulted in spiking after a delay (Fig. 15C). The intrinsic membrane currents observed in these cells did

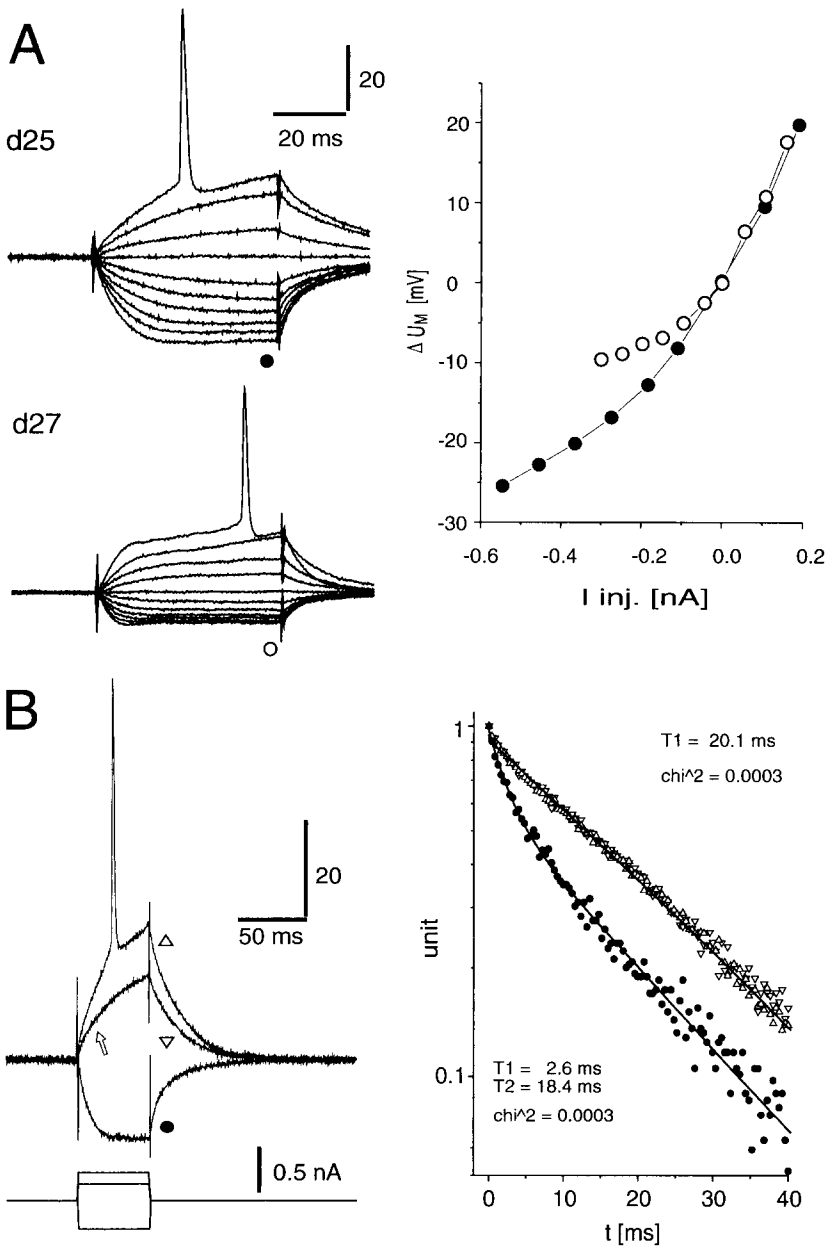

Fig. 11. Electrophysiological characteristics of striatal principal cells in cortex–striatum co-cultures. (A) Intracellular membrane potential responses to hyperpolarizing and depolarizing current pulses with equidistant amplitudes. Membrane potential values reached after 50 ms were plotted against current amplitudes used (right). The neurons from this cell class show a varying degree of "anomalous rectification" in the hyperpolarized range. (B) After sub- and suprathreshold depolarizing pulses, the decay to the resting potential shows a single component. After hyperpolarizing pulses the return of the membrane potential to the resting potential reveals the presence of an additional fast component. Note different time courses to reach similar amplitude deflections for the hyperpolarized and depolarized states, respectively (arrow).

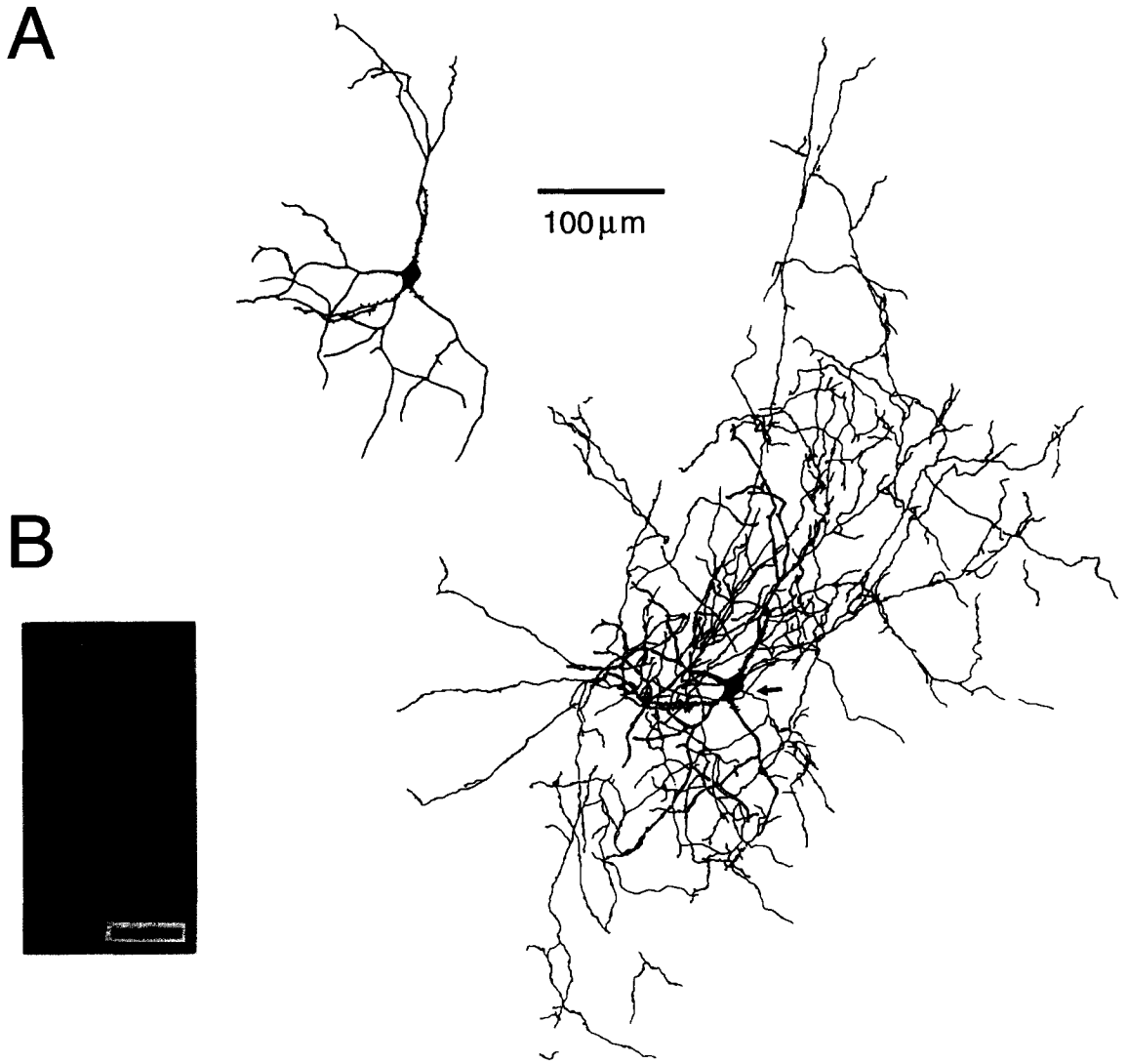

Fig. 12. (A) Morphology of the dendritic and axonal trees of a principal cell injected with neurobiotin. Only the largest spine-like protrusions at proximal dendrites are indicated. The axon (arrow) emanates from the cell body. Neurobiotin reconstruction. (B) Dendritic tree of striatal medium-spiny neuron at higher magnification (40 days *in vitro*, d40). Scale bar = 10 μm.

not lead to a depolarized, subthreshold state under conditions of spontaneous activity (Fig. 15D; see companion paper).

Striatal secondary type II neurons

Fifteen cells were identified as type II neurons. These neurons were characterized by their linear *I–V* characteristics and a very prominent AHP (Fig. 16A, Table 1). The membrane potential decay from depolarized subthreshold and suprathreshold levels showed a single component (Fig. 16B, C). Often, these neurons exhibited transient, subthreshold oscillations upon depolarization, resulting in doublet spikes with highly constant interspike intervals (Fig. 16D; see also the companion paper). They were characterized morphologically by a large elongated-polygonal cell body of $348 \pm 64\ \mu m^2$ ($n = 9$) and extended, sparsely branched smooth dendrites. When visualized, these neurons resembled striatal cholinergic interneurons (Figs 2F, 16E).

Further indications that type II neurons in the striatum are cholinergic neurons came from developmental studies. ChAT-positive neurons in the rat neostriatum undergo a shrinkage in cell body area during the fourth week *in vivo*.[51] Such a shrinkage might be paralleled by an increase in apparent input resistance and a decrease in apparent input capacitance (ratio between membrane time constant and apparent input resistance). Indeed, a comparison of type II cells at the end of the third week (18–21 days *in vitro*; 20 ± 1 days *in vitro*; $n = 9$) and at the beginning of the fourth week (22–27 days *in vitro*; 24 ± 2 days *in vitro*; $n = 6$) revealed clear changes.

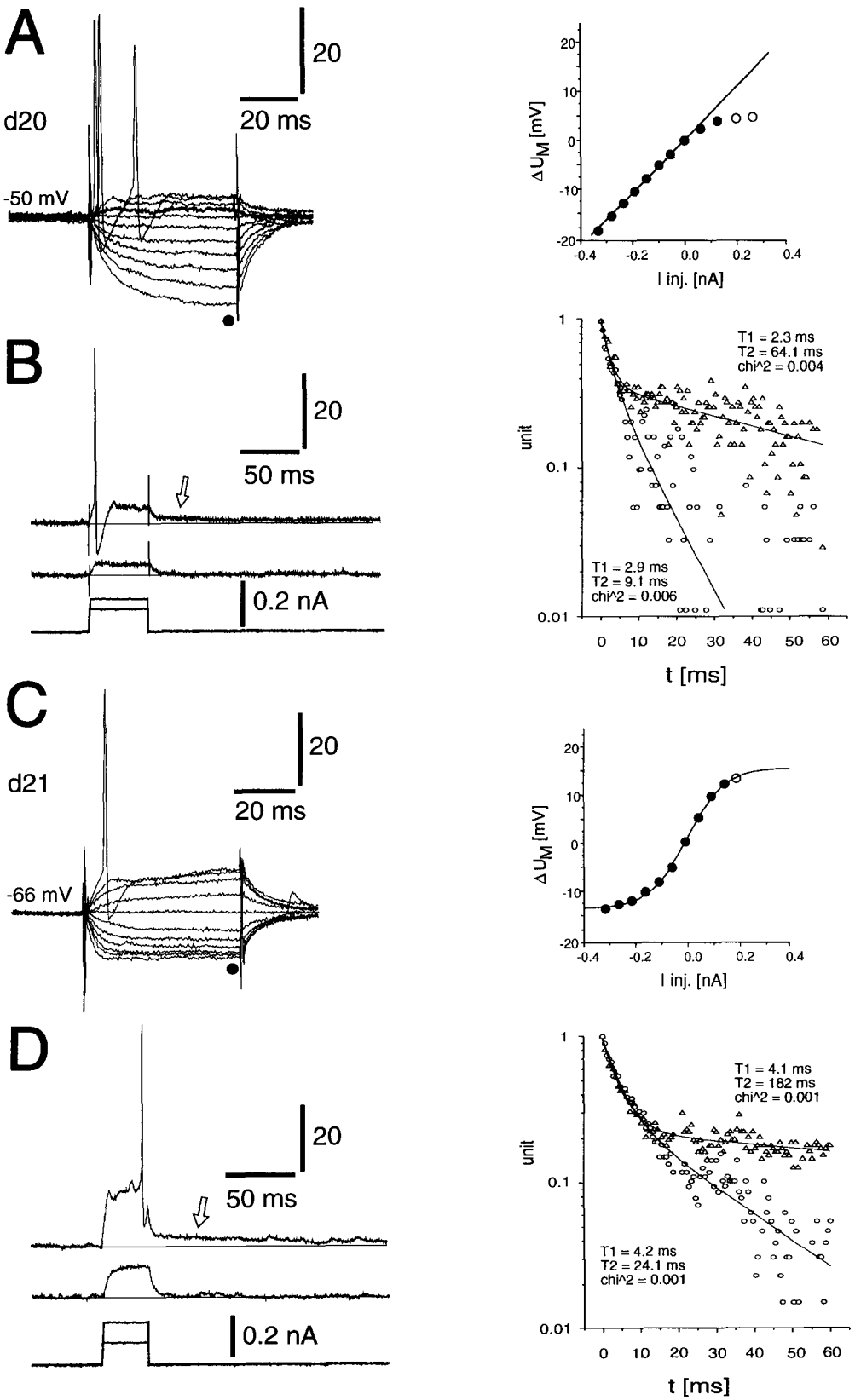

Fig. 13. Electrophysiological characteristics of striatal secondary type I neurons. (A) Type Ia neuron showing outward rectification in the subthreshold range but no inward rectification in the hyperpolarized range. Intracellular membrane potential responses to hyperpolarizing and depolarizing current pulses with equidistant amplitudes. Suprathreshold steady-state responses are indicated by open circles. (B) The decay time course changes when comparing subthreshold (middle trace; left) and suprathreshold (upper trace; left, arrow) responses to current pulses of different amplitudes. The semilogarithmic plot (right) reveals the existence of two components with different time constants in the subthreshold case ($T1$, $T2$; open circles). After the occurrence of a spike, the time constant of the fast component ($T1$) remains stable; however, the time constant of the slow component ($T2$) increases strongly (open triangles, right). (C) Intracellular membrane potential responses in a type Ib neuron to hyperpolarizing and depolarizing current pulses with equidistant amplitudes. The I–V diagram reveals a strongly non-linear steady-state behavior (see Table 2). Suprathreshold steady-state response is indicated by an open circle. (D) A similar protocol as shown in B again reveals that the occurrence of a spike predominantly changes the time constant of the slow component.

Table 3. Time constants of the fast (τ_1) and slow component (τ_2) in type Ia and Ib neurons (the two cell classes are not significantly different at the $P < 0.05$ level; Wilcoxon's rank sum

Decay time constant (ms)	Secondary type Ia	Cell number	Secondary type Ib	Cell number
τ_1	4.5 ± 1.1	9	4.7 ± 1.2	8
τ_2 (subthreshold)	14 ± 7	7	19 ± 4	8
τ_2 (after spike)	69 ± 44	9	67 ± 48	8
τ_2 (after burst)	—	—	590 ± 150	3

The apparent input resistance and the apparent input capacitance at the end of the third week were $39 \pm 17\ M\Omega$ and 0.23 ± 0.007 mF, respectively. During the fourth week the input resistance increased to $82 \pm 24\ M\Omega$ and the apparent input capacitance decreased to 0.12 ± 0.04 mF ($P < 0.005$; Wilcoxon's rank sum test). Similar changes could not be detected in the other cell classes and for other parameters.

DISCUSSION

Parvalbumin-positive neurons

Cortex. The distribution of parvalbumin-positive cells described for the cortical part in the co-cultures is very similar to the results obtained *in vivo* from parietal, somatosensory and primary motor cortex of the rat. Parvalbumin-positive cells were found in the rat and monkey in cortical layers II–VI, with a clear accumulation in the middle layers.[28,56,81,130] The laminar pattern shown in the parvalbumin stain indicates the presence of cortical layers in the organotypic co-culture. This is in accordance with earlier findings based on field potential reversal,[36] Nissl stain and fiber bundles[118] in single organotypic mouse cortex explants taken from early postnatal days.

The degree of overlap between parvalbumin-positive cells and GABAergic interneurons is not complete and changes with species and brain area examined (see e.g. Refs 39 and 111). Nevertheless, some comparisons with GABAergic interneuron classes in organotypic single cortex cultures can be made. In single cortices taken at age around P7 and cultured for several weeks, GABAergic bipolar and GABAergic "basket" cells are present.[25] Furthermore, a specific vasoactive intestinal polypeptide-positive, GABAergic class of bipolar interneurons situated in the upper cortical layers was shown to develop in single cortex slices taken into culture at P0–P2.[49,50] These VIP interneurons resemble very closely the parvalbumin-positive cell types described for the upper regions of the cortical tissue in the co-culture system.

Striatum. The strongly parvalbumin-positive cell type described for the adult rat striatum is a fusional-polygonal neuron with varicose dendrites, which strongly correlates with the striatal aspiny GABAergic interneuron.[30,35,78] In the co-culture system the morphological features of striatal strongly parvalbumin-positive cells closely match strongly parvalbumin-positive cells[35,78] and striatal GABAergic interneurons *in vivo*.[13,112] Thus, we conclude that the striatal aspiny GABAergic interneuron is expressed in cortex–striatum co-cultures.

Strongly parvalbumin-positive neurons showed a much more variable morphology than ChAT-positive cells in the co-culture. This heterogeneity in morphology might indicate further subclassifications,[67] as is the case in the hippocampus.[111] The average cell body area of these cells is comparable to that of intensively stained striatal parvalbumin-positive cells in adult rats *in vivo*[78] and of glutamate decarboxylase (GAD)-positive interneurons in single organotypic striatal cultures.[101]

In the striatal culture, single axons of parvalbumin-positive cells could be followed over long distances. In such cases, multiple boutons were often seen aligned to parvalbumin-negative cell bodies (Fig. 3B). Similar accumulations of parvalbumin-positive boutons have been reported *in vivo*.[78] Furthermore, in the co-cultures we were able to trace these accumulations of boutons with respect to the dendritic tree of the cell. Often, such "baskets" were found several hundred micrometers away from the dendritic tree. Thus, these neurons can transmit information between different striatal regions (see type I neurons and the companion paper).

In single organotypic single striatal cultures, GABA- and GAD-positive neurons have been described,[101] which the strongly parvalbumin-positive neurons described here resemble. However, in single organotypic cultures protospines are present on these neurons, indicating an immature state. In the present study strongly labeled striatal parvalbumin-positive neurons are morphologically indistinguishable from those described *in vivo*, and no protospines were observed (compare, for example, Figs 5 and 6 with Kita *et al.*[78] and Cowan *et al.*[35]). These differences suggest that cortical input influences the morphology of striatal GABAergic interneurons, altering it to a mature state. A functional role of cortical input onto striatal GABAergic interneurons is further supported by the high numbers of asymmetrical, probably cortical, synapses onto dendrites of these neurons *in vivo*.[73,83]

Apart from the strongly parvalbumin-positive cells, a large number of weakly stained cell bodies was also visible: weakly parvalbumin- and GAD-positive cell bodies in the adult striatum and in single organotypic striatal cultures are commonly considered to

be striatal principal neurons.[78,101] In the co-culture system, large striatal parvalbumin-positive cell bodies could, in some instances, be found (Fig. 2C), similar to findings reported for GAD-positive cells in single striatal cultures[101] and for GABA-positive cells *in vivo*.[103]

Choline acetyltransferase-positive neurons

The morphology of striatal ChAT-positive neurons in the co-cultures is remarkably similar to ChAT-positive neurons in the neostriatum of young[51] and adult[15,30,72,107,146] rats *in vivo* and in single organotypic striatal cultures *in vitro*.[101] The average cell body area of $327 \pm 99\ \mu m^2$ after 22 days in culture is similar to the value obtained from cholinergic neurons of three-week-old rats *in vivo* ($333 \pm 16\ \mu m^2$; corrected for shrinkage by 22%).[51] The relatively large area found here was also reported for the adult rat striatum *in vivo*.[107] In addition, large ChAT-positive neurons, contrasted by a majority of smaller, labeled neurons, have been reported in the adult striatum[4] and in single organotypic striatal cultures.[101]

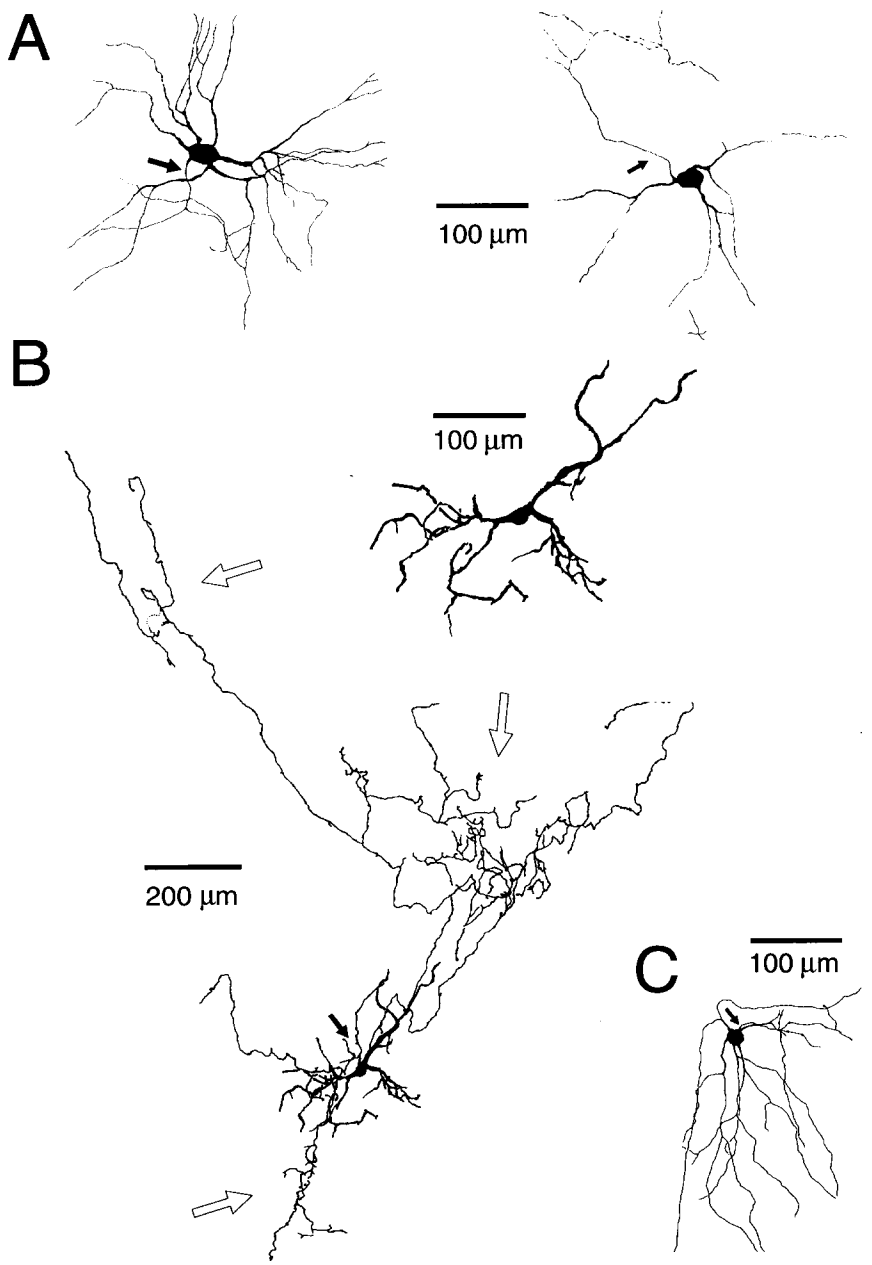

Fig. 14. Dendritic (A, B) and axonal (B) morphologies of secondary type I neurons. Arrows point to the axons emanating from the cell body. At least three regions of axonal branching distant from the dendritic field were revealed in one neuron (B; open arrows). (C) Reconstruction of the morphology of the secondary neuron type Ib with "principal cell"-like morphology (neurobiotin; compare with Fig. 2F, PC).

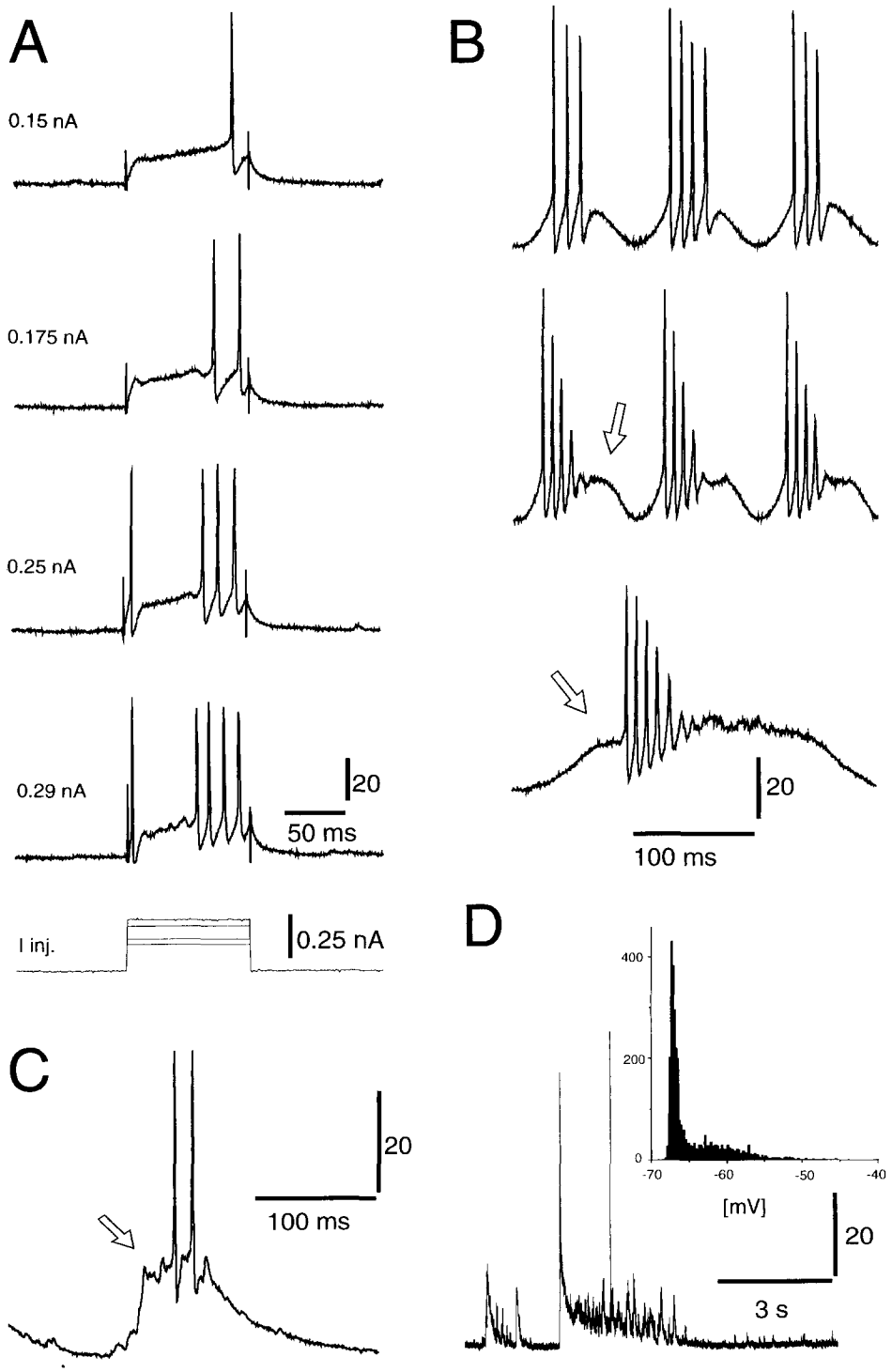

Fig. 15. Spiking cessation in striatal secondary type I neurons. (A) Intracellular membrane potential responses to depolarizing current pulses of increasing amplitudes (same neuron as in Fig. 13C). A characteristic delay in spike discharge upon depolarization can be observed. When current amplitude is further enhanced, a characteristic cessation in spike discharge occurs after the first spike. (B) Spiking behavior to sinusoidal current injections (upper trace: 10 Hz, 0.25 nA; middle trace: 10 Hz, 0.75 nA; lower trace: 3 Hz, 0.75 nA). Under conditions of strong input current, the regular spike amplitude decreases down to a level of complete spike blockade. At the end of such a "breakdown", the membrane potential seems to be dominated by strong outwardly rectifying currents (middle trace; arrow). By lowering the frequency it can be shown that the strong outwardly rectifying current(s) start before the occurrence of a spike (lower trace; arrow). (C) Delayed spike response to spontaneous synaptic activity, which is similar to the delayed response upon current injection at the cell body (different neuron than in A). (D) Spontaneous intracellular activity and corresponding membrane potential distribution from a secondary type Ib neuron (same neuron as in A). Membrane potential values were taken at 2 ms intervals.

ChAT-positive cells in the co-cultures were mainly restricted to the striatal part. In some instances, regions devoid of labeled cells were present. This indicates a partial heterogeneity of the striatal tissue; *in vivo*, striatal "patches" seem to be devoid of cholinergic, i.e. large aspiny, cell bodies.[3,65,93] The existence of a patch/matrix organization in the co-culture system would be in contrast to the situation in single organotypic striatal cultures, where, at the end of the third week, any postnatal patchy

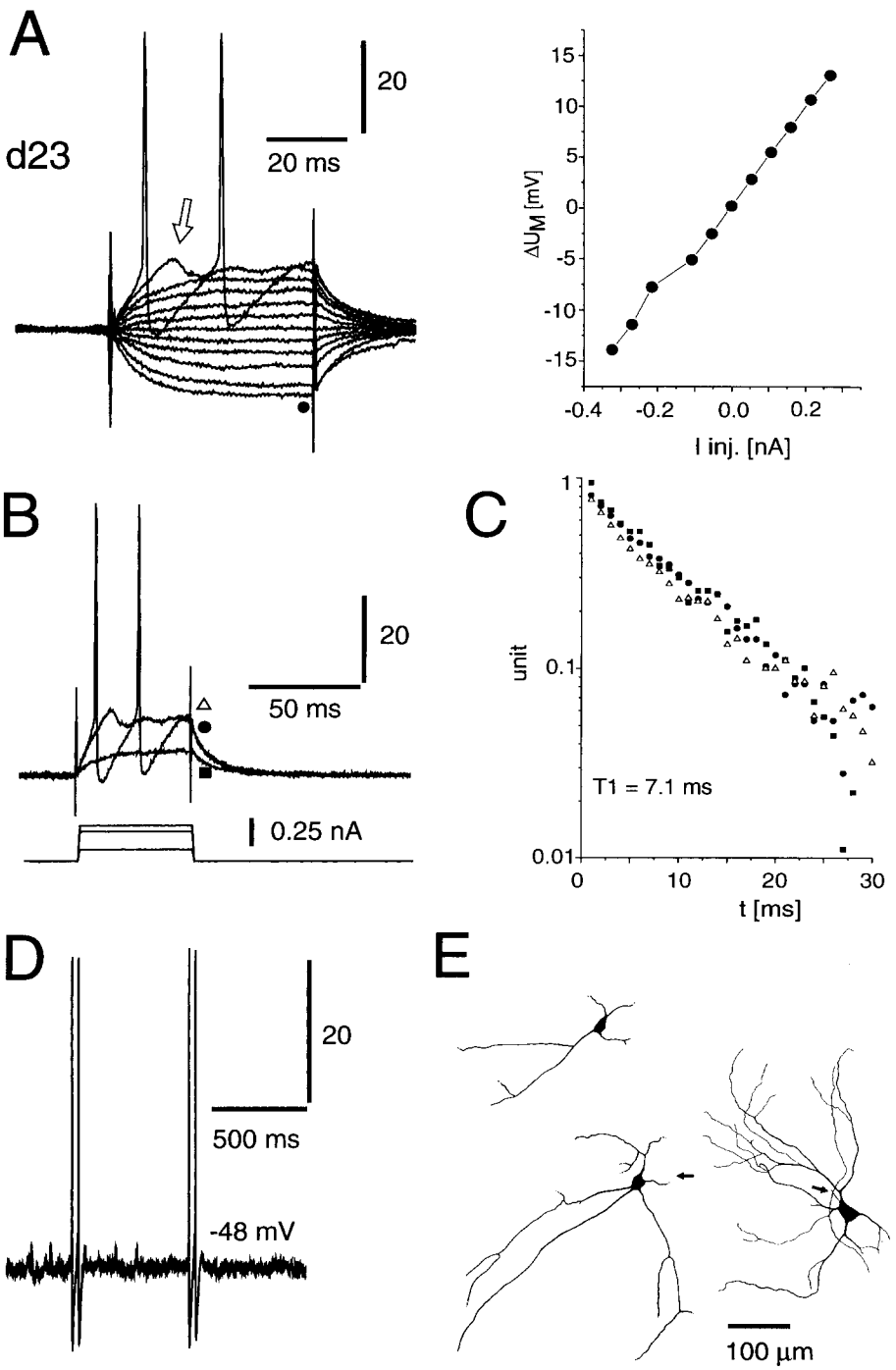

Fig. 16. Electrophysiological and morphological characteristics of striatal secondary type II neurons. (A) Intracellular membrane potential responses to hyperpolarizing and depolarizing current pulses with equidistant amplitudes. The *I–V* diagram reveals a linear steady-state behavior (right). (B, C) Membrane potential decay reveals a single component. No change in the decay time course is found after depolarizing sub- and suprathreshold current pulses (semilogarithmic plot; right). (D) Spontaneous spike discharge often occurred in doublet spikes. (E) Reconstruction of the morphology of secondary type II neurons (neurobiotin). Arrows point to the axons emanating from the cell bodies (compare also Fig. 2F, SC).

organization based on acetylcholinesterase or ChAT immunoreactivity disappears.[101]

In one preparation some ChAT-positive cells were found in the cortical tissue. These neurons probably originated in the cortical culture, as in the rat cortex ChAT-positive cells are present at low density.[58]

Calbindin-positive neurons

In the cortex the spatial distributions of calbindin- and parvalbumin-positive cells were inversely correlated corresponding to findings in the cortex of rats[28,116] and monkeys.[33,56] Strongly stained calbindin-positive cells were only present in small numbers at the border of the striatal tissue. The neuropil was devoid of labeled fibers; however, weakly stained medium-sized cell bodies were present. As we cultured striatal tissue mainly from dorsolateral and lateral regions, but not from ventromedial and ventral regions (see Experimental Procedures), our findings are in accordance with results obtained in the acute slice.[69]

Corticostriatal projection neurons

The most prominent corticostriatal projection neuron is characterized by its medium-sized cell body,[144] its small basal dendritic field, a sparsely branched apical dendrite and a huge axonal arborization in both the cortex and the striatum.[34,136] In the medial agranular cortex, this type of corticostriatal projection neuron is found in the lower part of layer III and superficial layer V.[136] In the somatosensory cortex, medium-sized corticostriatal projection cells are mainly situated in superficial layer V,[144] although some corticostriatal projection cells have been reported in layers II and III.[117]

In the co-culture system, corticostriatal projection neurons were found mainly in the lower part of the cortical culture, which most probably corresponds to layer V *in vivo*. A characteristic feature of these cells was their small basal dendritic tree and their sparsely branched or unbranched apical dendrite. This is probably a genuine finding for the following reasons. Firstly, a reduced dendritic tree size due to incomplete staining seems to be very unlikely, because of the intense stain of even finer, multiple branched axonal collaterals. Secondly, no change in morphology with longer exposure to DiI was observed. Thirdly, it is known that pyramidal cells in organotypic cortex cultures show a reduction in branching and an elongation of interbranch segments compared with pyramidal cells *in vivo*.[26] However, in organotypic visual cortex–visual cortex, visual cortex–thalamus[16,17,99] and visual cortex–tectum[80] co-cultures, cortical projection cell classes have been described, which also include large-sized pyramidal neurons with intensively branched basal and apical dendritic trees. Thus, we conclude that the population of projection cells revealed is a specific class of pyramidal cells similar to the class of medium-sized corticostriatal/corticocortical projection cells described *in vivo* for the medial agranular cortex.[34,136] The characteristic morphology and the laminar position of these projection neurons strongly suggests that the corticostriatal projection which develops in the co-culture system shares common features with the projection system *in vivo*. Such specificity in the development of internuclei projections is supported by findings in other co-culture systems.[16]

The cortex was densely labeled by axon collaterals from corticostriatal projection neurons. Besides collaterals spreading along cortical layers, collaterals running straight to the upper cortical border were also present. This indicates that corticostriatal projection neurons, in addition to transmitting information directly to the striatum, influence other cortical neurons within a single column and, through horizontal collaterals, across several columns.

The type of corticopyramidal tract projection cell which emits short axonal collaterals into the striatum[34,42,82] was not found in the co-culture system. Finely branched axons of short length sent to the striatal tissue might have escaped our analysis.

Electrophysiologically characterized cell types in the co-culture system

Cortical pyramidal neurons. Adult pyramidal neurons *in vivo* from supragranular layers are characterized by their inward rectification in the subthreshold range[59,91] (rat; slice) and the change in AHP after the first spike (Fig. 8B; compare guinea-pig[90]). Pyramidal cells from layer V are further distinguished by an inward rectification at very hyperpolarized levels and the rebound and hyperpolarization after hyper- and depolarizing current injections, respectively (rat; slice).[29,84,91] All these features were found in cortical pyramidal cells of the co-culture. We will now consider in more detail the various electrophysiological parameters.

Resting membrane potential. Cortical pyramidal cells in the co-culture system showed a 15–25 mV more positive resting potential than in the acute slice preparation.[2,10,32,40,59,84] We attribute this difference to the $[K^+]_o$ of 5.8 mM in our preparation and the spontaneous activity in the co-culture system.

Input resistance. The relatively high input resistance of pyramidal cells in the co-cultures is similar to findings in single organotypic[145] and dissociated[60] cortical cultures. The resistance is approximately four-fold larger than *in vivo* and approximately two-fold larger than in the acute slice preparation.[10,32,59,89] In single organotypic cortical cultures, pyramidal cells have a less dense arborization and a slightly reduced spine density compared to pyramidal cells *in vivo*.[26] Both effects should lead to a reduced membrane area of cultured neurons and may explain the increased input resistance seen in our preparation.

Spike wave form. The short spike width of cultured cortical neurons indicates the mature developmental stage[88,91] and is similar to the spike width found in

dissociated cortical cultures.[60] The absolute spike rise time in our preparation is lower than obtained by others in organotypic[145] and dissociated[60] cortical cultures. We attribute this difference to the low sampling rate and the averaging procedure used. The ratio between the rising and the falling rate of the action potential is similar to the ratios measured in acute slice preparation.[91] In contrast to young pyramidal neurons, adult neurons have a triphasic AHP: a short-lasting and a long-lasting AHP separated by a depolarization.[2,84,89] This feature is seen in the co-culture system at the end of the fourth week (Fig. 8C).

Morphology. Pyramidal cells in the co-cultures show typical morphological characteristics such as the cell body form and the basal and apical dendrites being covered with spines.

To summarize, cortical pyramidal neurons in the co-culture system show a similar degree of maturity as cortical neurons *in vivo* of similar age. However, cultured pyramidal cells have a higher input resistance than *in vivo*.

Cortical interneurons. The cortical interneuron described is similar to cortical interneurons in the rat[66,68] and fast spiking, cortical interneurons in the guinea-pig.[90] The spike width of 1 ms and two-fold higher rate of decrease of the spike than for pyramidal neurons found by us was also reported for inhibitory neurons in dissociated cortical cultures.[60] As the cortical interneuron was located in a layer expressing a dense band of parvalbumin-positive cells (cf. Fig. 1) it is probably of the parvalbumin-positive type. This view is supported by the very short time-to-peak of the AHP typical for parvalbumin-positive interneurons in rat prefrontal cortex.[2,66]

Striatal principal cells

Resting membrane potential and passive parameters. Principal cells were the most polarized cells in the co-culture (Table 1), which is in accordance with findings *in vivo*[24,113,126,138–140,143] and in acute slices *in vitro*.[7,23,75,79,96,97] The absolute resting membrane potential of principal neurons is strongly dependent on the extracellular potassium concentration.[7] Given the extracellular potassium concentration of 5.8 mM, the resting membrane potential we found is in good agreement with findings in adult rats *in vivo*[24,126] and in *in vitro* slice studies using similar $[K^+]_o$ concentrations.[7,23] Similar to the situation for pyramidal neurons, the input resistance is twice as large as *in vivo*[24,126] and in *in vitro* slice preparations.[69,79]

Steady-state non-linearity and spike wave form. The steady-state non-linearity described here for cultured principal cells is typical for principal cells *in vivo* and in acute slices.[7,22,23,69,79] The action potential width of unidentified striatal cells *in vivo*[24] and *in vitro*[23,69] is in the range of 1.0–1.5 ms. As pointed out by Kita *et al.*,[76] this value holds for the first spike in a burst, whereas subsequent spikes are broadened. Thus, the average spike half width of 1.5 ms reported here points to a mature spike. In comparison with striatal secondary neurons, principal cells showed a longer spike width and a smaller AHP, which is similar to the situation in the *in vitro* slice.[65]

Morphology. The cell body area of electrophysiologically identified principal cells matches that of the most abundant neuron type in the striatal culture (Fig. 5) and is similar to the cell body area reported for electrophysiologically identified and morphologically reconstructed rat principal cells.[11,65,108] The morphological features of cultured principal cells are typical for most principal cells *in vivo* and *in vitro*.[11,14,65,69,108] However, in contrast to the situation *in vivo*, spine-like protrusions can be found on the very proximal dendrites.

To summarize, the polarized resting membrane potential, the rectification characteristics, the small AHP, the small cell body size, the spiny dendritic tree and the densely branched axonal field are typical features of striatal GABAergic medium-spiny projection neurons (= principal cells), which are expressed in the co-culture system.

Striatal secondary cell types. A comparative analysis of the intracellular electrophysiological behavior of striatal interneurons is particularly difficult and is limited by the different methods and recording conditions used (whole-cell patch-clamp in immature slices[65,67] *in vivo* under various experimental conditions;[141] adult slice preparation[63]).

Striatal secondary type I neurons

Outward rectification. The outward rectification reported in this study refers to the first 50 ms after depolarization onset. In immature slices under "whole cell" patch conditions, striatal GABAergic interneurons expressed rectifications similar to those reported here.[67] In two other studies with similar large numbers of analysed interneurons,[63,141] neurons were sampled by chance and thus might be biased towards very large-sized cholinergic interneurons without outward rectification (see below).

Membrane potential decay from depolarized levels. The slow component was a very robust feature in all secondary cells of type I, regardless of their resting membrane potential. No differences were found regarding type Ia and Ib cells (Table 3). In the most intensive study on striatal GABAergic interneurons[67] these particular dynamics have not been reported, probably due to the method used.

Firing behavior. Secondary type I neurons expressed the most complex intrinsic membrane dynamics found in the co-culture system. We will show in the companion paper that these dynamics can explain the complex, but stereotypical firing patterns found in these neurons. The characteristic spike cessation seems to be robust against changes in the interior milieu, as it was also found in striatal GABAergic interneurons under "whole cell" patch conditions.[65,67]

Inward rectification at hyperpolarized levels. In type Ib neurons strong inward rectification was demonstrated at hyperpolarized levels. As type Ia neurons were relatively depolarized, such inward rectification might have gone undetected. We suggest that both types represent one single neuron type.

Morphology. The dendritic morphology of type I neurons was similar to the morphology of striatal strongly parvalbumin-positive interneurons, which are equivalent to GABAergic interneurons.[13,77,78,105,112] Furthermore, type I cells showed axonal arborizations at various different striatal regions outside their dendritic field. Similar, although incomplete, reconstructions of the dendritic and axonal fields were revealed for strongly parvalbumin-positive striatal cells (cf. Figs 3, 14). These dendritic and axonal arborizations described in this study correspond well with the common morphology of striatal GABAergic interneurons found in immature slices of the rat.[67]

Secondary type Ib cells with "principal cell"-like morphology. One type I cell showed a distinct "principal cell"-like morphology and a strong asymmetric dendritic tree (Fig. 14C), although its prominent outward rectification (Fig. 13C) separated this neuron from principal cells. However, principal cells with a sigmoid steady-state non-linearity have been reported in the caudate nucleus of the cat.[123]

Striatal secondary type II neurons

Resting membrane potential and passive membrane parameters. The high resting membrane potential of striatal type II cells is similar to the resting membrane potentials reported for large aspiny neurons *in vivo*,[141] the class of secondary neurons in acute slices[63] and the population of striatal cholinergic interneurons recorded under "whole-cell" patch conditions in immature rat slices.[67] However, the input resistance of type II cells is lower than in acute slice preparations[63,65,67] and in the anesthetized rat.[141] We attribute this low input resistance to the excitatory input these neurons receive in the co-culture system (see Ref. 107a). The linear steady-state membrane dynamics of type II cells within the first 50 ms have also been reported for large-sized,[63,65,141] cholinergic[67] striatal interneurons from acute preparations. In addition, strong inward rectification below -70 mV has been reported for striatal cholinergic[67] interneurons.[63,67] This rectification develops slowly on a time scale of several hundreds of milliseconds. The high resting potential of type II cells, the low input resistance and the short-lasting current pulses we used might explain why this rectification was not seen in our experiments.

Spike wave form. The spike wave form with its prominent AHP is in accordance with findings on striatal interneurons from the acute slice preparations[63,65,67] and *in vivo*.[141] The time to maximum AHP in type II cells is much shorter than reported for the slice preparation using the "whole-cell" patch approach.[65,67] As this AHP is mediated by the opening of $I_{K[Ca]}$,[67] the disturbance of the internal calcium concentration might account for this difference. Nevertheless, type II neurons showed slower time to peak AHP than type I neurons, which agrees with findings in acute immature slices.[67]

Morphology. The average cell body area of type II neurons is similar to that obtained for the ChAT-positive neurons in the co-cultures and for cholinergic[67] interneurons reported in acute striatal slices.[63,65,67] It is slightly lower than for the striatal interneurons reported by Wilson *et al.*[141] Type II cells were characterized by a large, slightly elongated cell body with long, smooth and sparsely branched dendrites. These morphological features are similar to the ones observed in the ChAT-positive neurons in the co-culture system. In combined Golgi and immunohistochemical ChAT studies *in vivo* it was shown that these morphological features are typical for striatal ChAT-positive neurons in the rat.[15] We conclude that striatal type II neurons in the co-cultures are striatal cholinergic interneurons.

Other striatal interneuron classes. Besides the two interneuron classes reported here, a variety of other small to medium-sized interneuron classes are present in the striatum.[8,38,124,128] Among these classes, at least NADPH-diaphorase-positive interneurons[38,67,133] have cell body sizes[133] which make them likely to be sampled by our visual selection criterion.[67] The complex and very characteristic spiking behavior of these cells under hyperpolarized conditions makes it easy to discriminate them from other cell classes.[67]

CONCLUSIONS

From anatomy and physiology we conclude that organotypic cortex–striatum co-cultures show strong similarities with the cortex and the striatum *in vivo*. These similarities apply to the macroscopic organization as well as to the various cortical and striatal cell classes studied. In the companion paper we will demonstrate that this high degree of similarity can be extended to the neural interaction at the network level.

Acknowledgements—We thank Volker Staiger and Inge Hemmasi for skilful technical assistance, Heike Hoffmann and Katharina Braun for advice regarding the immunohistochemical procedures, and Valentino Braitenberg and Jeff Wickens for inspiring discussions. Additional support was received from the German "Bundesministerium für Forschung und Technologie" (BMFT).

REFERENCES

1. Aldridge J. W. and Gilman S. (1991) The temporal structure of spike trains in the primate basal ganglia: afferent regulation of bursting demonstrated with precentral cerebral cortical ablation. *Brain Res.* **543,** 123–138.

2. Alonso A. and Klink R. (1993) Differential electroresponsiveness of stellate and pyramidal-like cells of entorhinal cortex layer II. *J. Neurophysiol.* **70,** 128–143.
3. Aosaki T., Kimura M. and Graybiel A. M. (1992) Physiologically identified tonically active neurons of primate striatum lie in the matrix compartment. *IBAGS IV, Fourth Triennial Meeting of the International Basal Ganglia Society* 3 (Abstract).
4. Armstrong D. M., Saper C. B., Levey A., Wainer B. H. and Terry R. D. (1983) Distribution of cholinergic neurons in rat brain: demonstrated by the immunohistochemical localization of choline acetyltransferase. *J. comp. Neurol.* **216,** 53–68.
5. Armstrong-James M. and Fox K. (1988) Evidence for a specific role for cortical NMDA receptors in slow-wave sleep. *Brain Res.* **451,** 189–196.
6. Baimbridge K. G., Celio M. R. and Rogers J. H. (1992) Calcium-binding proteins in the nervous system. *Trends Neurosci.* **15,** 303–308.
7. Bargas J., Galarraga E. ,and Aceves J. (1988) Electrotonic properties of neostriatal neurons are modulated by extracellular potassium. *Expl Brain Res.* **72,** 390–398.
8. Bennet B. D. and Bolam J. P. (1993) Characterization of calretinin-immunoreactive structures in the striatum of the rat. *Brain Res.* **609,** 137–148.
9. Berendse H. W., Galis-de Graaf Y. and Groenewegen H. J. (1992) Topographical organization and relationship with ventral striatal compartments of prefrontal corticostriatal projections in the rat. *J. comp. Neurol.* **316,** 314–347.
10. Bindman L. J., Meyer T. and Prince C. A. (1988) Comparison of the electrical properties of neocortical neurons in slices *in vitro* and in the anesthetized rat. *Expl Brain Res.* **69,** 489–496.
11. Bishop G. A., Chang H. T. and Kitai S. T. (1982) Morphological and physiological properties of neostriatal neurons: an intracellular horseradish peroxidase study in the rat. *Neuroscience* **7,** 179–191.
12. Bolam J. P. and Izzo P. N. (1988) The postsynaptic targets of substance P immunoreactive terminals in the rat neostriatum with particular reference to identified spiny striatonigral neurons. *Expl Brain Res.* **70,** 361–377.
13. Bolam J. P., Powell J. F., Wu J.-Y. and Smith A. D. (1985) Glutamate decarboxylase-immunoreactive structures in the rat neostriatum: a correlated light and electron microscopic study including a combination of Golgi-impregnation with immunocytochemistry. *J. comp. Neurol.* **237,** 1–20.
14. Bolam J. P., Somogyi P., Totterdell S. and Smith A. D. (1981) A second type of striatonigral neuron: a comparison between retrogradely labeled and Golgi-stained neurons at the light and electron microscopic levels. *Neuroscience* **11,** 2141–2157.
15. Bolam J. P., Wainer B. H. and Smith A. D. (1984) Characterization of the cholinergic neurons in the rat neostriatum. A combination of choline acetyltransferase immunocytochemistry, Golgi impregnation and electron microscopy. *Neuroscience* **12,** 711–718.
16. Bolz J., Novak N., Götz M. and Bonhoeffer T. (1990) Formation of target-specific neuronal projections in organotypic slice cultures from rat visual cortex. *Nature* **346,** 359–362.
17. Bolz J., Novak N. and Staiger V. (1992) Formation of specific afferent connections in organotypic slice cultures from rat visual cortex cocultured with lateral geniculate nucleus. *J. Neurosci.* **12,** 3054–3070.
18. Braun K., Scheich H., Heizmann C. W. and Hunziker W. (1991) Parvalbumin and calbindin-D28k immunoreactivity as developmental markers of auditory and vocal motor nuclei of the zebra finch. *Neuroscience* **40,** 853–869.
19. Brown L. L. and Feldman S. M. (1993) The organization of the somatosensory activity in the dorsolateral striatum of the rat. In *Chemical Signaling in the Basal Ganglia* (eds Arbuthnott G. W. and Emson P. C.), vol. 99, pp. 237–250. *Progress in Brain Research.* Elsevier, Amsterdam.
20. Brown R. G. and Marsden C. D. (1990) Cognitive function in Parkinson's disease: from description to theory. *Trends Neurosci.* **13,** 21.
21. Cajal S. R. (1911) *Histologie du Système Nerveux.* A. Maloine, Paris.
22. Calabresi P., Mercuri N., Stanzione P., Stefani A. and Bernardi G. (1987) Intracellular studies on the dopamine-induced firing inhibition of neostriatal neurons *in vitro*: evidence for D1-receptor involvement. *Neuroscience* **20,** 757–771.
23. Calabresi P., Mercuri N. B. and Bernardi G. (1990) Synaptic and intrinsic control of membrane excitability of neostriatal neurons. II. An *in vitro* analysis. *J. Neurophysiol.* **63,** 663–675.
24. Calabresi P., Mercuri N. B., Stefani A. and Bernardi G. (1990) Synaptic and intrinsic control of membrane excitability of neostriatal neurons. I. An *in vivo* analysis. *J. Neurophysiol.* **63,** 651–662.
25. Cäser M., Bonhoeffer T. and Bolz J. (1989) Cellular organization and development of slice cultures from rat visual cortex. *Expl Brain Res.* **477,** 234–244.
26. Cäser M. and Schüz A. (1992) Maturation of neurons in neocortical slice cultures. A light and electron microscopic study on *in situ* and *in vivo* material. *J. Hirnforsch.* **33,** 429–443.
27. Celio M. R. (1986) Parvalbumin in most gamma-aminobutyric acid-containing neurons of the rat cerebral cortex. *Science* **231,** 995–997.
28. Celio M. R. (1990) Calbindin d-28k and parvalbumin in the rat nervous system. *Neuroscience* **35,** 375–475.
29. Chagnac-Amitai Y., Luhmann H. J. and Prince D. A. (1990) Burst generating and regular spiking layer 5 pyramidal neurons of rat neocortex have different morphological features. *J. comp. Neurol.* **296,** 598–613.
30. Chang H. T. and Kita H. (1992) Interneurons in the rat striatum: relationships between parvalbumin neurons and cholinergic neurons. *Brain Res.* **574,** 307–311.
31. Chang H. T., Wilson C. J. and Kitai S. T. (1981) Single neostriatal efferent axons in the globus pallidus: a light and electron microscopic study. *Science* **213,** 915–918.
32. Connors B. W., Malenka R. C. and Silva L. R. (1988) Two inhibitory postsynaptic potentials, and GABAa and GABAb receptor-mediated responses in neocortex of rat and cat. *J. Physiol., Lond.* **406,** 433–468.
33. Cote P. Y., Sadikot A. F. and Parent A. (1991) Complementary distribution of calbindin D-28k and parvalbumin in the basal forebrain and midbrain of the squirrel monkey. *Eur. J. Neurosci.* **3,** 1316–1329.
34. Cowan R. L. and Wilson C. J. (1994) Spontaneous firing patterns and axonal projections of single cortico-striatal neurons in the rat medial agranular cortex. *J. Neurophysiol.* **71,** 17–32.
35. Cowan R. L., Wilson C. J., Emson P. C. and Heizmann C. W. (1990) Parvalbumin-containing GABAergic interneurons in the rat neostriatum. *J. comp. Neurol.* **302,** 197–205.

36. Crain S. M. and Bornstein M. B. (1964) Bioelectric activity of neonatal mouse cerebral cortex during growth and differentiation in tissue culture. *Expl Neurol.* **10,** 425–450.
37. Crawford G. D., Correa L. and Salvaterra P. M. (1982) Interaction of monoclonal antibodies with mammalian choline transferase. *Proc. natn. Acad. Sci. U.S.A.* **79,** 7031–7035.
38. Dawson T. M., Bredt D. S., Fotuhi M., Hwang P. M. and Snyder S. H. (1991) Nitric oxide synthetase and neuronal NADPH-diaphorase are identical in brain and peripheral tissues. *Proc. natn. Acad. Sci. U.S.A.* **88,** 7797–7801.
39. Defelipe J., Hendry S. H. C. and Jones E. G. (1989) Visualization of chandelier cells axons by parvalbumin immunoreactivity in monkey cerebral cortex. *Proc. natn. Acad. Sci. U.S.A.* **86,** 2093–2097.
40. Deisz R. A., Fortin G. and Zieglgänsberger W. (1991) Voltage dependence of excitatory postsynaptic potentials of rat neocortical neurons. *J. Neurophysiol.* **65,** 371–382.
41. DeLong M. R. (1990) Primate models of movement disorders of basal ganglia origin. *Trends Neurosci.* **13,** 281–285.
42. Donoghue J. P. and Kitai S. T. (1981) A collateral pathway to the neostriatum from cortico-fugal neurons of the rat sensory-motor cortex: an intracellular HRP-study. *J. comp. Neurol.* **201,** 1–13.
43. Eckenstein F. and Thoenen H. (1982) Production of specific antisera and monoclonal antibodies to choline acetyltransferase: characterization and use for identification of cholinergic neurons. *Eur. molec. Biol. Org. J.* **1,** 363–368.
44. Furman G. G. (1965) Comparison of models for subtractive and shunting lateral inhibition in receptor-neuron fields. *Kybernetik* **2,** 257–274.
45. Gähwiler B. H. (1981) Organotypic monolayer cultures of nervous tissue. *J. Neurosci. Meth.* **4,** 329–342.
46. Gähwiler B. H. (1989) Organotypic cultures of neural tissue. *Trends Neurosci.* **11,** 484–489.
47. Gerfen C. R. (1992) The neostriatal mosaic: multiple levels of compartmental organization. *Trends Neurosci.* **15,** 133–139.
48. Godement P., Vanselow J., Thanos S. and Bonhoeffer F. (1987) A study in developing visual systems with a new method of staining neurons and their processes in fixed tissue. *Development* **101,** 697–713.
49. Götz M. and Bolz J. (1989) Development of vasoactive intestinal polypeptide (VIP)-containing neurons in organotypic slice cultures from rat visual cortex. *Neurosci. Lett.* **107,** 6–11.
50. Götz M. and Bolz J. (1992) Formation and preservation of cortical layers in slice cultures. *J. Neurobiol.* **23,** 783–802.
51. Gould E., Woolf N. J. and Butcher L. L. (1991) Postnatal development of cholinergic neurons in the rat: I. Forebrain. *Brain Res. Bull.* **27,** 767–789.
52. Hadeler K. P. (1974) On theory of lateral inhibition. *Kyb* **14,** 161–165.
53. Hadeler K. P. and Kuhn D. (1987) Stationary states of the Hartline–Ratliff model. *Biol. Cybern.* **56,** 411–417.
54. Hall R. D. and Lindholm E. P. (1974) Organization of motor and somatosensory neocortex in the albino rat. *Brain Res.* **73,** 249–255.
55. Heizmann C. W. (1984) Parvalbumin, an intracellular calcium-binding protein: distribution, properties and possible roles in mammalian cells. *Experientia* **40,** 910–921.
56. Hendrickson A. E., Vanbrederode J. F. M., Mulligan K. A. and Celio M. R. (1991) Development of the calcium-binding proteins parvalbumin and calbindin in monkey striate cortex. *J. comp. Neurol.* **307,** 626–646.
57. Horikawa K. and Armstrong W. E. (1988) A versatile means of intracellular labeling: injection of biocytin and its detection with avidin conjugates. *J. Neurosci. Meth.* **25,** 1–11.
58. Houser C. R., Crawford G. D., Salvaterra P. M. and Vaughn J. E. (1985) Immunocytochemical localization of choline acetyltransferase in rat cerebral cortex: a study of cholinergic neurons and synapses. *Brain Res.* **234,** 17–34.
59. Howe J. R., Sutor B. and Zieglgänsberger W. (1987) Baclofen reduces post-synaptic potentials of rat cortical neurons by an action other than its hyperpolarizing action. *J. Physiol., Lond.* **384,** 539–569.
60. Huettner J. E. and Baughman R. W. (1988) The pharmacology of synapses formed by identified corticocollicular neurons in primary cultures of rat visual cortex. *J. Neurosci.* **8,** 160–175.
61. Huguenard J. R., Hamill O. P. and Prince D. A. (1988) Development changes in Na^+ conductance in rat neocortical neurons: appearance of a slowly inactivating component. *J. Neurophysiol.* **59,** 778–795.
62. Jaeger D., Kita H. and Wilson C. J. (1994) Surround inhibition among projection neurons is weak or nonexistent in the rat neostriatum. *J. Neurophysiol.* **72,** 2555–2558.
63. Jiang Z.-G. and North R. A. (1991) Membrane properties and synaptic responses of rat striatal neurons *in vitro*. *J. Physiol., Lond.* **443,** 533–553.
64. Katayama Y., Miyazaki S. and Tsubokawa T. (1981) Electrophysiological evidence favoring intracaudate axon collaterals of GABAergic caudate output neurons in the cat. *Brain Res.* **216,** 180–186.
65. Kawaguchi Y. (1992) Large aspiny cells in the matrix of the rat neostriatum *in vitro*—physiological identification, relation to the compartments and excitatory postsynaptic currents. *J. Neurophysiol.* **67,** 1669–1682.
66. Kawaguchi Y. (1993) Groupings of non-pyramidal cells with specific physiological and morphological characteristics in rat frontal cortex. *J. Neurophysiol.* **69,** 416–431.
67. Kawaguchi Y. (1993) Physiological, morphological, and histochemical characterization of three classes of interneurons in rat neostriatum. *J. Neurosci.* **13,** 4908–4923.
68. Kawaguchi Y. and Kubota Y. (1993) Correlation of physiological subgroupings of non-pyramidal cells with parvalbumin- and calbindin-D28K-immunoreactive neurons in layer V of rat frontal cortex. *J. Neurophysiol.* **70,** 387–396.
69. Kawaguchi Y., Wilson C. J. and Emson P. (1989) Intracellular recording of identified neostriatal patch and matrix spiny cells in a slice preparation preserving cortical inputs. *J. Neurophysiol.* **62,** 1052–1068.
70. Kemp J. M. and Powell T. P. S. (1970) The cortico-striate projection in the monkey. *Brain* **93,** 525–546.
71. Kemp J. M. and Powell T. P. S. (1971) The structure of the caudate nucleus of the cat: light and electron microscopy. *Phil. Trans. R. Soc. Lond.* **262,** 383–401.
72. Kimura H., McGeer P. L., Peng F. and McGeer E. G. (1980) Choline acetyltransferase-containing neurons in rodent brain demonstrated by immunohistochemistry. *Science* **208,** 1057–1059.

73. Kita H. (1993) GABAergic circuits of the striatum. In *Chemical Signaling in the Basal Ganglia* (eds Arbuthnott G. W. and Emson P. C.), vol. 99, pp. 51–72. *Progress in Brain Research*. Elsevier, Amsterdam.
74. Kita H. and Armstrong W. (1991) A biotin-containing compound *N*-(2-aminoethyl)biotinamide for intracellular labeling and neuronal tracing studies: comparison with biocytin. *J. Neurosci. Meth.* **37,** 141–150.
75. Kita H., Kita T. and Kitai S. T. (1985) Active membrane properties of rat neostriatal neurons in an *in vitro* slice preparation. *Expl Brain Res.* **60,** 54–62.
76. Kita H., Kita T. and Kitai S. T. (1985) Regenerative potentials in rat neostriatal neurons in an *in vitro* slice preparation. *Expl Brain Res.* **60,** 63–70.
77. Kita H. and Kitai S. T. (1988) Glutamate decarboxylase immunoreactive neurons in rat neostriatum: their morphological types and populations. *Brain Res.* **447,** 346–352.
78. Kita H., Kosaka T. and Heizmann C. W. (1990) Parvalbumin-immunoreactive neurons in the rat neostriatum: a light and electron microscopic study. *Brain Res.* **536,** 1–15.
79. Kita T., Kita H. and Kitai S. T. (1984) Passive electrical membrane properties of rat neostriatal neurons in an *in vitro* slice preparation. *Brain Res.* **300,** 129–139.
80. Klauer S. (1991) The corticotectal projection of the rat established in organotypic culture. *NeuroReport* **2,** 569–572.
81. Kosaka T., Heizmann C. W. and Fujita S. C. (1992) Monoclonal antibody-473 selectively stains a population of GABAergic neurons containing the calcium-binding protein parvalbumin in the rat cerebral-cortex. *Expl Brain Res.* **89,** 109–114.
82. Landry P., Wilson C. J. and Kitai S. T. (1984) Morphological and electrophysiological characteristics of pyramidal tract neurons in the rat. *Expl Brain Res.* **57,** 177–190.
83. Lapper S. R., Smith Y., Sadikot A. F., Parent A. and Bolam J. P. (1992) Cortical input to parvalbumin-immunoreactive neurons in the putamen of the squirrel monkey. *Brain Res.* **580,** 215–224.
84. Larkman A. and Mason A. (1990) Correlations between morphology and electrophysiology of pyramidal neurons in slices of rat visual cortex. I. Establishment of cell classes. *J. Neurosci.* **10,** 1407–1414.
85. Lehmann J. and Langer S. Z. (1983) The striatal cholinergic interneuron: synaptic target of dopaminergic terminals. *Neuroscience* **10,** 1105–1120.
86. Lighthall J. W., Park M. R. and Kitai S. T. (1981) Inhibition in slices of rat neostriatum. *Brain Res.* **212,** 182–187.
87. Lu E. J. and Brown W. J. (1977) The developing caudate nucleus in the euthyroid and hypothyroid rat. *J. comp. Neurol.* **171,** 261–284.
88. Luhmann H. J. and Prince D. A. (1991) Postnatal maturation of the GABAergic system in rat neocortex. *J. Neurophysiol.* **65,** 247–263.
89. Mason A. and Larkman A. (1990) Correlations between morphology and electrophysiology of pyramidal neurons in slices of rat visual cortex. II. Electrophysiology. *J. Neurosci.* **10,** 1415–1428.
90. McCormick D. A., Connors B. W., Lighthall J. W. and Prince D. A. (1985) Comparative electrophysiology of pyramidal and sparsely spiny stellate neurons of the neocortex. *J. Neurophysiol.* **54,** 782–806.
91. McCormick D. A. and Prince D. A. (1987) Post-natal development of electrophysiological properties of rat cerebral cortical pyramidal neurons. *J. Physiol., Lond.* **393,** 743–762.
92. McGeorge A. J. and Faull R. L. M. (1989) The organization of the projection from the cerebral cortex to the striatum in the rat. *Neuroscience* **29,** 503–537.
93. Meredith G. E., Blank B. and Groenewegen H. J. (1989) The distribution and compartmental organization of the cholinergic neurons in nucleus accumbens of the rat. *Neuroscience* **31,** 327–345.
94. Miller R., Wickens J. R. and Beninger R. J. (1990) Dopamine D-1 and D-2 receptors in relation to reward and performance: a case for the D-1 receptor as a primary site for therapeutic action of neuroleptic drugs. *Prog. Neurobiol.* **34,** 143–183.
95. Misgeld U., Frotscher M. and Wagner A. (1984) Identification of projecting neurons in rat neostriatal slices. *Brain Res.* **299,** 367–370.
96. Misgeld U., Wagner A. and Ohno T. (1982) Depolarizing IPSPs and depolarization by GABA of rat neostriatum cells *in vitro*. *Expl Brain Res.* **45,** 108–114.
97. Misgeld U., Weiler M. H. and Bak I. J. (1980) Intrinsic cholinergic excitation in the rat neostriatum: nicotinic and muscarinic receptors. *Expl Brain Res.* **39,** 401–409.
98. Morishita I. and Yajima A. (1972) Analysis and simulation of networks of mutually inhibiting neurons. *Kybernetik* **11,** 154–165.
99. Novak N. and Bolz J. (1993) Formation of specific efferent connections in organotypic slice cultures from rat visual cortex cocultured with lateral geniculate nucleus and superior colliculus. *Eur. J. Neurosci.* **5,** 15–24.
100. Oertel W. H. and Mugnaini E. (1984) Immunocytochemical studies of GABAergic neurons in rat basal ganglia and their relationships to other neuronal systems. *Neurosci. Lett.* **47,** 233–238.
101. Ostergaard K. (1993) Organotypic slice cultures of the rat striatum. I. A histochemical and immunohistochemical study of acetylcholinesterase, choline acetyltransferase, glutamate decarboxylase and GABA. *Neuroscience* **53,** 679–693.
102. Ostergaard K., Schou J. P., Gähwiler B. H. and Zimmer J. (1989) Tyrosine hydroxylase immunoreactive neurons in organotypic slice cultures of the rat striatum and neocortex. *Expl Brain Res.* **83,** 357–365.
103. Otterson O. P. and Storm-Mathisen J. (1984) Glutamate- and GABA-containing neurons in the mouse and rat brain, as demonstrated with a new immunocytochemical technique. *J. comp. Neurol.* **229,** 374–392.
104. Park M. R., Lighthall J. W. and Kitai S. T. (1980) Recurrent inhibition in the rat neostriatum. *Brain Res.* **194,** 359–369.
105. Pasik P., Pasik T., Holstein G. R. and Hamori J. (1988) GABAergic elements in the neuronal circuits of monkey neostriatum: a light and electron microscopic immunocytochemical study. *J. comp. Neurol.* **270,** 157–170.
106. Paxinos G. and Watson C. (1982) *The Rat Brain in Stereotaxic Coordinates*. Academic Press, Sydney.
107. Phelps P. E., Houser C. R. and Vaughn J. E. (1985) Immunocytochemical localization of choline acetyltransferase within the rat neostriatum: a correlated light and electron microscopic study of cholinergic neurons and synapses. *J. comp. Neurol.* **238,** 286–307.
107a. Plenz D. and Aertsen A. (1995) Neural dynamics in cortex–striatum co-cultures—II. Spatiotemporal characteristics of neuronal activity. *Neuroscience* **70,** 893–924.
108. Preston R. J., Bishop G. A. and Kitai S. T. (1980) Medium spiny neuron projection from the rat striatum: an intracellular horseradish peroxidase study. *Brain Res.* **183,** 253–263.

109. Rebec G. V. and Curtis S. D. (1988) Reciprocal zones of excitation and inhibition in the neostriatum. *Synapse* **2,** 633–635.
110. Reep R. L., Corwin J. V., Hashimoto A. and Watson R. T. (1987) Efferent connections of the rostral portion of medial agranular cortex in rats. *Brain Res. Bull.* **19,** 203–221.
111. Ribak C. E., Nitsch R. and Seress L. (1990) Proportion of parvalbumin-positive basket cells in the GABAergic innervation of pyramidal and granule cells of the rat hippocampal formation. *J. comp. Neurol.* **300,** 449–461.
112. Ribak C. E., Vaughn J. E. and Roberts E. (1979) The GABA neurons and their axon terminals in rat corpus striatum as demonstrated by GAD immunohistochemistry. *J. comp. Neurol.* **187,** 261–284.
113. Richardson T. L., Miller J. J. and McLennan H. (1977) Mechanisms of excitation and inhibition in the nigrostriatal system. *Brain Res.* **127,** 219–234.
114. Schmidt-Kastner R., Meller D. and Eysel U. T. (1992) Immunohistochemical changes of neuronal calcium-binding proteins parvalbumin and calbindin-D-28k following unilateral deafferentiation in the rat visual system. *Expl Neurol.* **117,** 230–246.
115. Schüz A. and Palm G. (1989) Density of neurons and synapses in the cerebral cortex of the mouse. *J. comp. Neurol.* **286,** 442–455.
116. Schwab C., Bruckner G. and Hartig W. (1992) Parvalbumin and calbindin immunoreactivity in the rat brain. A double-immunolabeling method. *Acta histochem.* **S42,** 277–281.
117. Schwab M., Agid Y., Glowinski J. and Thoenen H. (1977) Retrograde axonal transport of ^{125}I-tetanus toxin as a tool for tracing fiber connections of the rostral part of the rat neostriatum. *Brain Res.* **126,** 211–224.
118. Seil F. J., Kelly M. J. III and Leiman A. L. (1974) Anatomical organization of cerebral neocortex in tissue culture. *Expl Neurol.* **45,** 435–450.
119. Seite R., Vuillet-Luciani J., Vio M. and Cataldo C. (1977) Sur la présence d'inclusions nucléares dans certain neurones du noyau caudé du rat: répartition, fréquence et organisation ultrastructurale. *Biol. Cell* **30,** 73–76.
120. Sladeczek F., Recasens M. and Bockaert J. (1988) A new mechanism for glutamate receptor action: phosphoinositide hydrolysis. *Trends Neurosci.* **11,** 545–549.
121. Smith A. D. and Bolam J. P. (1990) The neural network of the basal ganglia as revealed by the study of synaptic connections of identified neurones. *Trends Neurosci.* **13,** 259–265.
122. Somogyi P., Bolam J. P. and Smith A. D. (1981) Monosynaptic cortical input and local axon collaterals of identified striatonigral neurons. A light and electron microscopic study using the Golgi-peroxidase transport degeneration procedure. *J. comp. Neurol.* **195,** 567–584.
123. Sugimori M., Preston R. J. and Kitai S. T. (1978) Response properties and electrical constants of caudate nucleus neurons in the cat. *J. Neurophysiol.* **41,** 1662–1676.
124. Takagi H., Somogyi P. and Smith A. D. (1983) Fine structural studies on a type of somatostatin-immunoreactive neuron and its synaptic connections in the neostriatum: a correlated light and electron microscopic study. *J. comp. Neurol.* **214,** 1–16.
125. Tashiro Y., Sugimoto T., Hattori T., Uemura Y., Nagatsu I., Kikuchi H. and Mizuno N. (1989) Tyrosine hydroxylase-like immunoreactive neurons in the striatum of the rat. *Neurosci. Lett.* **97,** 6–10.
126. Tepper J. M. and Trent F. (1993) *In vivo* studies of the postnatal development of rat neostriatal neurons. In *Chemical Signaling in the Basal Ganglia* (eds Arbuthnott G. W. and Emson P. C.), vol. 99, pp. 35–50. *Progress in Brain Research.* Elsevier, Amsterdam.
127. Thanos S. and Bonhoeffer F. (1987) Axonal arborization in the developing chick retinotectal system. *J. comp. Neurol.* **261,** 155–164.
128. Theriault E. and Landis D. M. D. (1987) Morphology of striatal neurons containing VIP-like immunoreactivity. *J. comp. Neurol.* **256,** 1–13.
129. Tigges M. and Tigges J. (1991) Parvalbumin immunoreactivity of the lateral geniculate nucleus in adult rhesus monkeys after monocular eye enucleation. *Vis. Neurosci.* **6,** 375–382.
130. Van Brederode J. F. M., Helliesen M. K. and Hendrickson A. E. (1991) Distribution of the calcium-binding proteins parvalbumin and calbindin-D28k in the sensorimotor cortex of the rat. *Neuroscience* **44,** 157–171.
131. Van Eden C. G. and Uylings H. B. M. (1985) Cytoarchitectonic development of the prefrontal cortex in the rat. *J. comp. Neurol.* **241,** 253–267.
132. Varjú D. (1962) Vergleich zweier Modelle für laterale Inhibition. *Kybernetik* **2,** 200–208.
133. Vincent S. R., Johansson O., Hökfelt T., Skirboll L., Elde R. P., Terenius L., Kimmel J. and Goldstein M. (1983) NADPH-diaphorase: a selective histochemical marker for striatal neurons containing both somatostatin- and avian pancreatic polypeptide (APP)-like immunoreactivities. *J. comp. Neurol.* **217,** 252–263.
134. Welker C. (1971) Microelectrode delineation of fine grain somatotopic organization of SmI cerebral neocortex in albino rat. *Brain Res.* **26,** 259–275.
135. Wickens J. R., Alexander M. E. and Miller R. (1991) Two dynamic modes of striatal function under dopaminergic–cholinergic control: simulation and analysis of a model. *Synapse* **8,** 1–12.
136. Wilson C. J. (1987) Morphology and synaptic connections of crossed corticostriatal neurons in the rat. *J. comp. Neurol.* **263,** 567–580.
137. Wilson C. J. (1992) Dendritic morphology, inward rectification and the functional properties of neostriatal neurons. In *Single Neuron Computation* (eds McKenna T., Davis J. and Zornetzer S. F.), pp. 141–171. Academic Press, San Diego.
138. Wilson C. J. (1993) The generation of natural firing patterns in neostriatal neurons. In *Chemical Signaling in the Basal Ganglia* (eds Arbuthnott G. W. and Emson P. C.), pp. 277–298. *Progress in Brain Research.* Elsevier, Amsterdam.
139. Wilson C. J., Chang H. T. and Kitai S. T. (1983) Origins of post synaptic potentials evoked in spiny neostriatal projection neurons by thalamic stimulation in the rat. *Expl Brain Res.* **51,** 217–226.
140. Wilson C. J., Chang H. T. and Kitai S. T. (1983) Disfacilitation and long-lasting inhibition of neostriatal neurons in the rat. *Expl Brain Res.* **51,** 227–235.
141. Wilson C. J., Chang H. T. and Kitai S. T. (1990) Firing patterns and synaptic potentials of identified giant aspiny interneurons in the rat neostriatum. *J. Neurosci.* **10,** 508–519.
142. Wilson C. J. and Groves P. M. (1980) Fine structure and synaptic connections of the common spiny neuron of the rat neostriatum: a study employing intracellular injection of horseradish peroxidase. *J. comp. Neurol.* **194,** 599–615.

143. Wilson C. J. and Groves P. M. (1981) Spontaneous firing patterns of identified spiny neurons in the rat neostriatum. *Brain Res.* **220,** 67–80.
144. Wise S. P. and Jones E. G. (1977) Cells of origin and terminal distribution of descending projections of the rat somatic sensory cortex. *J. comp. Neurol.* **175,** 129–158.
145. Wolfson B., Gutnick M. J. and Baldino F. (1989) Electrophysiological characteristics of neurons in neocortical explant cultures. *Expl Brain Res.* **76,** 122–130.
146. Yelnik J., Percheron G., Francois C. and Garnier A. (1993) Cholinergic neurons of the rat and primate striatum are morphologically different. In *Chemical Signaling of the Basal Ganglia* (eds Arbuthnott G. W. and Emson P. C.), vol. 99, pp. 25–34. *Progress in Brain Research.* Elsevier, Amsterdam.

(*Accepted* 28 *July* 1995)